

Seasonal photoacclimation in the North Pacific Transition Zone

Gregory L Britten^{1,1}, Christine Padalino^{1,1}, Gaël Forget^{1,1}, and Michael J. Follows^{2,2}

¹Massachusetts Institute of Technology

²MIT

November 30, 2022

Abstract

The Transition Zone Chlorophyll Front (TZCF) is a dynamic region of elevated chlorophyll concentrations in the Northeast Pacific that migrates from a southern winter (February) extent of approximately 30°N to a northern summer (August) extent of approximately 40°N. The transition zone has been highlighted as important habitat for marine animals and fisheries. We re-examine the physical and biological drivers of seasonal TZCF variability using a variety of remote sensing, reanalysis, and in-situ datasets. Satellite-based remote sensing estimates of chlorophyll and carbon concentrations show that seasonal TZCF migration primarily reflects a seasonal increase in the chlorophyll to carbon ratio, rather than changes in phytoplankton carbon. We use our data compilation to demonstrate how the seasonality of light and nutrient fluxes decouple chlorophyll and carbon seasonality at the transition zone latitudes. Seasonal mixed-layer-averaged light availability is positively correlated with carbon and negatively correlated with chlorophyll through the transition zone, while climatological nitrate profiles show that chlorophyll to carbon ratios are facilitated by wintertime nitrate entrainment. These empirical results are consistent with physiological data and models describing elevated chlorophyll to carbon ratios in low light, nutrient-replete environments, demonstrating the importance of latitudinal structure in interpreting seasonal chlorophyll dynamics at the basin scale.

1 Seasonal photoacclimation in the North Pacific Transition Zone

2 Gregory L. Britten^{1,†}, Christine Padalino^{1,2†}, Gaël Forget¹, Michael J. Follows¹

3 ¹Program in Atmospheres, Oceans, and Climate, Massachusetts Institute of Technology

4 ²Department of Chemical Engineering, Massachusetts Institute of Technology

5

6 Corresponding author: Gregory L. Britten (gbritten@mit.edu)

7 †Both authors contributed equally

8 **Key Points:**

- 9 • Seasonal variations in North Pacific chlorophyll show a distinct latitudinal structure in
10 phase and magnitude
- 11 • Chlorophyll concentrations are negatively correlated with carbon concentrations in the
12 transition zone (30-40°N)
- 13 • Latitudinally varying nutrient and light supply drive chlorophyll and carbon covariation
14 via photoacclimation

15 **Abstract**

16 The Transition Zone Chlorophyll Front (TZCF) is a dynamic region of elevated chlorophyll
17 concentrations in the Northeast Pacific that migrates from a southern winter (February) extent of
18 approximately 30°N to a northern summer (August) extent of approximately 40°N. The
19 transition zone has been highlighted as important habitat for marine animals and fisheries. We
20 re-examine the physical and biological drivers of seasonal TZCF variability using a variety of
21 remote sensing, reanalysis, and *in-situ* datasets. Satellite-based remote sensing estimates of
22 chlorophyll and carbon concentrations show that seasonal TZCF migration primarily reflects a
23 seasonal increase in the chlorophyll to carbon ratio, rather than changes in phytoplankton carbon.
24 We use our data compilation to demonstrate how the seasonality of light and nutrient fluxes
25 decouple chlorophyll and carbon seasonality at the transition zone latitudes. Seasonal mixed-
26 layer-averaged light availability is positively correlated with carbon and negatively correlated
27 with chlorophyll through the transition zone, while climatological nitrate profiles show that
28 chlorophyll to carbon ratios are facilitated by wintertime nitrate entrainment. These empirical
29 results are consistent with physiological data and models describing elevated chlorophyll to
30 carbon ratios in low light, nutrient-replete environments, demonstrating the importance of
31 latitudinal structure in interpreting seasonal chlorophyll dynamics at the basin scale.
32

33 **Plain Language Summary**

34 Satellite-observed marine chlorophyll concentrations are regularly interpreted as phytoplankton
35 carbon. However, the chlorophyll content of cells can vary due to several environmental factors,
36 thus complicating the interpretation of satellite-observed chlorophyll variability. In this study, we
37 examine the relationship between chlorophyll and phytoplankton carbon in the Northeast Pacific
38 – a region that has been highlighted as important habitat for marine animals. We find that
39 satellite-observed chlorophyll seasonality is strongly correlated with light and nutrient
40 availability but relatively uncorrelated with phytoplankton carbon due to changes in the
41 chlorophyll to carbon ratio. Deep winter mixed layers are the primary physical factor driving the
42 seasonal cycle in light and nutrient availability. These results provide a new perspective on
43 marine ecosystem productivity in the Northeast Pacific and demonstrate how latitudinal
44 differences in the seasonality of light and nutrient fluxes connect chlorophyll and carbon
45 dynamics at the basin scale.
46

47 **1 Introduction**

48 The North Pacific Transition Zone Chlorophyll Front (TZCF) is a basin-scale chlorophyll feature
49 noted in early satellite observations of ocean colour (Glover et al., 1994). The front exhibits
50 marked seasonality, moving from a summertime northern position at approximately 40°N, to a
51 wintertime southern position at approximately 30°N (Figure 1; Follett et al., 2021). The
52 transition zone (30-40°N) has been repeatedly highlighted as a congregation area for marine
53 animals and fisheries (Block et al., 2011; Hazen et al., 2013; Kappes et al., 2010; Polovina et al.,
54 2017; Xu et al., 2017). Tagging data, where animals are fitted with geo-locators, have shown
55 migratory and feeding behaviors throughout the transition zone, including commercially

56 important tuna (Polovina et al., 2017; Xu et al., 2017), seabirds (Block et al., 2011; Kappes et al.,
57 2010), and a variety of other marine animals (Block et al., 2011; Hazen et al., 2013).

58 Since early satellite observations, several studies have investigated the physical, chemical, and
59 biological drivers of TZCF variability, with authors noting the uniqueness of the apparent
60 wintertime productivity maximum at mid-latitudes (Ayers & Lozier, 2010; Bograd et al., 2004;
61 Chai et al., 2003; Glover et al., 1994; Le et al., 2019; Polovina et al., 2001, 2017). Glover &
62 McClain (1994) and Chai et al. (2003) suggested that deep winter mixed layers entrain nitrate and
63 drive the apparent wintertime productivity maximum, while Ayers & Lozier (2010) and Le et al.
64 (2019) suggested a stronger role for southward Ekman transport of nitrate.

65 Implicit in these earlier studies of TZCF dynamics is the assumption that the observed
66 chlorophyll variability corresponds to changes in phytoplankton carbon, while not considering
67 potential seasonal variations in chlorophyll to carbon ratios. Like other mid- and high-latitude
68 environments, the transition zone is characterized by large seasonal cycles in surface irradiance
69 and mixed layer depth which drives low wintertime light availability and elevated nutrient fluxes
70 to the mixed layer. The seasonal mixed layer cycle acts reduces light supply due to the
71 exponential extinction of light with depth while entraining nutrients if deep mixed layer
72 penetrate a strongly sloping nutricline (Evans et al., 1985). Physiological data and models show
73 that nutrient-replete, low light environments will increase the ratio of chlorophyll to carbon via
74 photoacclimation (Behrenfeld et al., 2016; Geider et al., 1996, 1998; Inomura et al., 2020; Laws
75 & Bannister, 1980; Westberry et al., 2008).

76 Behrenfeld et al., (2005) and others (e.g. Graff et al., 2016) leveraged correlations between
77 satellite-observed backscatter and phytoplankton carbon to demonstrate physiologically
78 interpretable decoupling of phytoplankton carbon and chlorophyll in response to light and
79 nutrient availability. From these relationships, we expect the North Pacific TZCF chlorophyll
80 signal to, in part, reflect photoacclimation responses to seasonal variations in light and nutrient
81 availability rather than variations in the underlying phytoplankton carbon. We test this
82 expectation by studying the latitudinal structure of surface chlorophyll and carbon variations
83 using a variety of remote sensing, reanalysis, and *in-situ* datasets. We disentangle the role of
84 photoacclimation in the observed TZCF chlorophyll dynamics by quantifying relationships
85 between chlorophyll concentrations, carbon concentrations, net primary productivity, light
86 availability, and mixed layer depths over the seasonal cycle. We examine these relationships
87 across latitudes to identify the unique chlorophyll cycle in the transition zone. These results will
88 help better understand ecosystem productivity in the North Pacific and improve our
89 interpretation of the mid-latitude satellite chlorophyll record.

90

91 **2 Methods**

92 We assembled a variety of remote sensing, reanalysis, and *in-situ* datasets to examine the
93 latitudinal structure of chlorophyll and carbon variations and the dynamics of photoacclimation
94 at the TZCF. Satellite remote sensing estimates of surface chlorophyll concentrations, carbon
95 concentrations, net primary productivity, surface photosynthetically active radiation (PAR), and
96 the diffuse attenuation coefficient (k_d) were obtained from the Oregon State Ocean Productivity
97 database (<http://sites.science.oregonstate.edu/ocean.productivity/>). These estimates have been
98 gap-filled for missing observations due to cloud cover according to the algorithm described at
99 http://orca.science.oregonstate.edu/gap_fill.php. Chlorophyll concentrations are based on the

100 Generalized Inherent Optical Property Algorithm (GIOP) using MODIS observations (Werdell et
 101 al., 2013). Carbon concentrations are based on backscatter coefficients estimated via the GIOP
 102 algorithm, modeled via the functions given in Behrenfeld et al., (2005) and Westberry et al.,
 103 (2008). We also repeated analyses using chlorophyll and carbon concentrations derived from the
 104 alternative Garver-Siegel-Maritorena (GSM) ocean color inversion algorithm (Maritorena et al.,
 105 2002) to ensure the consistency of results across inversion products. Net primary productivity
 106 was taken from four models that differ in their parameterization of phytoplankton growth: the
 107 vertically generalized productivity model (VGPM; Behrenfeld & Falkowski, 1997), the carbon-
 108 based productivity model (CBPM; Westberry et al., 2008), the Eppley vertically generalized
 109 productivity model (EPVGPM;
 110 <http://sites.science.oregonstate.edu/ocean.productivity/eppley.model.php>), and the Carbon,
 111 Absorption, and Fluorescence Euphotic-resolving model (CAFÉ; Silsbe et al., 2016). Surface
 112 PAR and k_d are estimated from MODIS observations (Son & Wang, 2015).

113 Reanalysis datasets of mixed layer depth were obtained from the simple ocean data assimilation
 114 product (SODA; version SODA3 12.2; available at <https://www.soda.umd.edu/>) and the Hybrid
 115 Coordinate Ocean Model (HyCOM; hindcast version GLBu0.08; available at
 116 <http://sites.science.oregonstate.edu/ocean.productivity>). SODA mixed layers were linearly
 117 interpolated from the original five-day interval to an eight-day interval to match the satellite and
 118 HyCOM datasets obtained from the Oregon State Productivity Database. We obtained mixed
 119 layer estimates from Argo based on the methods of Holte et al., (2017)
 120 (<http://mixedlayer.ucsd.edu/>). In the supplementary material we demonstrate a high correlation
 121 between SODA, HyCOM, and Argo mixed layer estimates (**Supplementary Figure S1**),
 122 indicating robustness across mixed layer depth products. All satellite and reanalysis datasets
 123 were bilinearly interpolated onto a common 0.5° grid. Climatological nitrate observations were
 124 taken from the World Ocean Atlas, version WOA2018 (Garcia et al., 2019). Mixed layer-
 125 averaged irradiance was calculated according to

$$126 \quad \bar{I} = \frac{1}{z_{ml}} \int_{z_{ml}}^0 I(z) dz = \frac{1}{k_d z_{ml}} I_0 e^{-k_d z_{ml}} (1 - e^{-k_d z_{ml}}),$$

127 where $I(z)$ is the scalar irradiance at depth z , k_d is the diffuse attenuation coefficient, z_{ml} is the
 128 depth of the mixed layer, and I_0 is the PAR incident at the sea surface. Entrainment nitrate fluxes
 129 into the mixed layer during mixed layer deepening were calculated according to

$$130 \quad F_N = \frac{dz_{ml}}{dt} (N_0 - N_{ml}),$$

131 where $\frac{dz_{ml}}{dt}$ is the entrainment velocity, N_0 is the nitrate concentration one meter below the mixed
 132 layer according to a linear interpolation of World Ocean Atlas nitrate profiles, and N_{ml} is the mixed
 133 layer-averaged nitrate concentration.

134 To investigate the latitudinal structure of chlorophyll and carbon dynamics, we binned
 135 observations according to six latitude bands across the Northeast Pacific, defined by longitudinal
 136 bounds of -180°W to -115°W . Latitudinal bands were defined by the intervals $0-10^\circ\text{N}$, $10-20^\circ\text{N}$,
 137 $20-30^\circ\text{N}$, $30-40^\circ\text{N}$, $40-50^\circ\text{N}$, $50-60^\circ\text{N}$. The western bound of -180°W was adopted to avoid
 138 influence of the western boundary current which imparts stochastic variability on the physical
 139 and chemical properties compared to the more stable latitudinal structure observed in the central
 140 and eastern reaches of the basin.

141 **3 Results**

142 *3.1 Covariation between chlorophyll and carbon*

143 The seasonal TZCF migration is readily observed by comparing chlorophyll maps for the months
144 of August and February (**Figure 1a,d**). August corresponds to the month of the maximum
145 northward extent at approximately 40°N, while February corresponds to the month of maximum
146 southward extent at approximately 30°N. Transition zone chlorophyll concentrations are elevated
147 three- to five-fold during the February chlorophyll maximum, relative to August. While February
148 is the month of maximum transition zone chlorophyll, concentrations are elevated over the
149 months of January-February-March which we hereafter refer to as transition zone winter.

150 Climatological maps demonstrate that February transition zone chlorophyll does not spatially
151 correlate to carbon concentrations across the basin (**Figure 1**). The transition zone shows no
152 appreciable increase in February carbon concentrations relative to August. February carbon
153 concentrations are also depressed to the north and south of the transition zone, in contrast to
154 chlorophyll which remains elevated to the north. The seasonal decoupling between chlorophyll
155 and carbon becomes clear in the climatological distribution of the chlorophyll to carbon ratio
156 (**Figure 1c,f**), where ratios are elevated roughly five-fold in winter from the transition zone
157 northward. Primary productivity models also disagree on the magnitude and spatial pattern of
158 wintertime transition zone productivity with no consistent spatial correlation with chlorophyll
159 (**Supplementary Figure S2**). Notably, the two productivity models that include
160 photoacclimation processes (CBPM and CAFÉ) estimate productivity south of the transition
161 zone to be more than double that of productivity models that do not include photoacclimation
162 (VGPM and Epply VGPM), again reflecting the decoupling of chlorophyll and carbon, here with
163 consequences for satellite-based productivity estimates.

164 The temporal dynamics of chlorophyll and carbon concentration time series clearly demonstrate
165 the latitudinal dependence of covariation between the two variables (**Figure 2**). Over the
166 seasonal cycle, chlorophyll concentrations in the transition zone are negatively correlated with
167 carbon concentrations ($r=-0.40$, **Figure 2c**). Negative correlations between chlorophyll and
168 carbon extend from 10-40°N, with the strongest negative correlation at 20-30°N ($r=-0.77$; **Figure**
169 **2d**). However, mean transition zone chlorophyll concentrations are several-fold higher than more
170 southern latitudes with a seasonal chlorophyll range of approximately 0.2 mgChl/m³,
171 highlighting the strength of the TZCF signal. Across latitudes, the seasonal correlation between
172 chlorophyll and productivity is also negative in the transition zone when averaging over four
173 primary productivity models ($r=-0.11$), with positive correlations between chlorophyll and
174 productivity at more northern and southern latitudes (**Supplementary Figure S3**). Across years,
175 negative correlations between chlorophyll and carbon are driven by a consistent offset in the
176 timing of their respective seasonal maxima, reflecting the chlorophyll peak in photoacclimated
177 low light conditions (**Figure 3**). All latitudes show an average lag between chlorophyll and
178 carbon maxima, with chlorophyll consistently peaking prior to carbon. The average lag across
179 latitudes is 90 days with a standard deviation of 95 days. The most consistent lag was found in
180 the transition zone, with a mean offset of 93 days and a standard deviation of 25 days across
181 years (**Figure 3**). Taken together, the negative correlations between transition zone chlorophyll
182 and carbon concentrations demonstrate the unique latitudinal structure of the chlorophyll cycle

183 across the North Pacific. The transition zone exhibits a high-amplitude chlorophyll cycle that is
184 largely independent of variations in phytoplankton carbon.

185 *3.2 Relationships with mixed layer depth and light availability*

186 The seasonal covariation of chlorophyll and carbon across latitude can be interpreted in terms of
187 latitude-specific responses to seasonal mixed layer depth variability and the resulting impact on
188 nutrient and light availability (**Figure 4**). Across latitudes, we find a consistently negative
189 relationship between mixed layer depth and carbon, with the strength of the relationship
190 decreasing southward (**Figure 4a-f**). In contrast, we find both positive and negative correlations
191 between mixed layer depth and chlorophyll across latitudes, with the largest positive slope in the
192 transition zone (**Figure 4i**). The consistent positive slope of the transition zone chlorophyll
193 relationship combines with a large range of seasonal mixed layer depths (20-145m) to yield a
194 transition zone chlorophyll cycle that is well predicted from a linear relationship with mixed
195 layer depth.

196 The correlation of mixed layer and light availability is shown in **Figure 5**. Large seasonal cycles
197 in surface irradiance and mixed layer depth are apparent at mid- and high-latitudes (**Figure 5a-**
198 **b**). The mean surface irradiance (around which the seasonal cycle oscillates) decreases
199 northward, with the summer maximum surface irradiance at 50-60°N roughly equal to
200 wintertime light availability in the tropics. Combining surface irradiance, mixed layer depth, and
201 satellite estimates of the light attenuation coefficient k_d , we find that the largest seasonal cycle in
202 mixed layer-averaged irradiance occurs in the transition zone, with a climatological seasonal
203 amplitude of approximately $170\mu\text{Mol quanta/m}^2/\text{s}$ and a wintertime light availability less than
204 $10\mu\text{Mol quanta/m}^2/\text{s}$ (**Figure 5c**). The minimal light availability in the transition zone winter
205 thus approaches the minimum compensation irradiance of photosynthesis (Geider et al., 1986;
206 Venables & Moore, 2010), highlighting the severe light limitation experienced by the wintertime
207 transition zone phytoplankton community.

208 The distinct responses of transition zone carbon and chlorophyll to mixed layer depth and light
209 availability are shown spatially by mapping the seasonal correlation coefficients across the basin
210 (**Figure 6**). The correlation of mixed layer depth vs. carbon concentration is negative across most
211 of the basin, with a band of weaker correlations in the transition zone (**Figure 6a**). Conversely,
212 correlations of mixed layer depth vs. chlorophyll are weak across much of the basin, except for
213 the band of strong negative correlations across the transition zone (**Figure 6b**). These patterns
214 further demonstrate that deepening winter mixed layers drive increases in chlorophyll
215 concentrations in the transition zone that are uncorrelated with variations in carbon. In terms of
216 mixed layer-averaged irradiance, we see weak positive correlations with carbon north of 20°N (r
217 ~ 0.20) and weak negative correlations southward ($r \sim -0.10$; **Figure 6c**). In contrast to carbon
218 and consistent with photoacclimation, chlorophyll strongly correlates with mixed layer-averaged
219 irradiance throughout the transition zone, with correlations between -0.5 and -0.7 (**Figure 6d**).
220 Zonally-averaged correlations reiterate this picture, showing diverging responses of carbon and
221 chlorophyll with respect to mixed layer depth and mixed layer-averaged irradiance in the
222 transition zone (**Figure 7**). We note that the correlation analysis was repeated using the
223 alternative mixed layer reanalysis from SODA (**Supplementary Figures S4 and S5**). We found

224 no appreciable difference in the magnitudes or spatial structure of the calculated correlations,
 225 indicating robustness in these relationships across mixed layer depth estimates.

226 Re-expressing relationships between light, carbon, and chlorophyll in terms of the chlorophyll to
 227 carbon ratio (Chl:C) reveals a strong nonlinear association between Chl:C and mixed layer-
 228 averaged irradiance, driven by nonlinear increases in Chl:C at the lowest light availability
 229 (**Figure 8**). The relationship between Chl:C and mixed layer-averaged irradiance is well-
 230 described by a negative exponential with light supply, like those described previously based on
 231 physiological principles (Behrenfeld et al., 2005; Graff et al., 2016; Jackson et al., 2017;
 232 Sathyendranath et al., 2020). The nonlinear response of Chl:C occurs in the light-limited regime
 233 encountered during transition zone winter.

234 *3.2 Mixed layer driven nutrient availability*

235 Deepening mixed layers can also act to entrain nutrients as deepening mixed layers penetrate
 236 layers of elevated nutrient concentrations. The resulting nutrient supply can then further enhance
 237 chlorophyll to carbon ratios due to the nitrogen requirement of chlorophyll and light harvesting
 238 protein synthesis, as faster growth rates require more chlorophyll for a given light level (Geider
 239 et al., 1998; Inomura et al., 2020). The entrainment nitrate flux is composed of the entrainment
 240 velocity from deepening mixed layers $\frac{dz_{ml}}{dt}$ and the nitrate gradient at the base of the mixed layer.

241 We find significant seasonality in entrainment velocity from 20°N and northward, with a
 242 maximum velocity that increases with latitude (**Figure 9a-b**). Similar latitudinal patterns are
 243 found in the mean nitrate gradient at the base of the mixed layer, with the mean gradient
 244 increasing northward beyond the equatorial latitudes (**Figure 9c**). The seasonal cycle in the
 245 subsurface nitrate gradient shows a more distinct latitudinal pattern. Nitrate uptake in the spring
 246 and summer drives the gradient from 20-40°N near zero in summer. This pattern contrasts with
 247 latitudes to the north and south of 20-40°N where spring and summer nitrate depletion is less
 248 severe. The entrainment velocity and nitrate gradient combine to yield a seasonal cycle of
 249 entrainment nitrate flux with an amplitude that increases with latitude (**Figure 9d**). Wintertime
 250 nitrate flux exceeds 30 mmol/m²/month north of 40°N and exceeds 10 mmol/m²/month in the
 251 transition zone, while remaining several fold lower southward. These results demonstrate that the
 252 transition zone latitudes of 30-40°N is the most southern latitude to receive a significant
 253 wintertime nitrate entrainment flux, consistent with arguments of Glover et al., (1994).

254 To ensure robustness of our results, we repeated all chlorophyll and carbon analyses above using
 255 estimates from the alternative GSM ocean colour inversion algorithm (Maritorena et al., 2002).
 256 Although low latitude GSM chlorophyll concentration magnitudes were slightly higher than
 257 GIOP estimates and low latitudes carbon slightly higher, the seasonality in the two inversions
 258 was highly consistent, reproducing the correlations reported above. All results using GSM
 259 estimates are reported in the Supplemental Information (Figures S6-10).

260 **4 Discussion**

261 *4.1 Photoacclimation as a primary driver of wintertime transition zone chlorophyll*

262 The observed negative covariation of chlorophyll and carbon in the transition zone, and its
 263 relationships with light and nutrient availability, demonstrate photoacclimation as a primary

264 driver of chlorophyll variability in the TZCF. Consistent with earlier satellite-based (Behrenfeld
265 et al., 2005) and physiological (Behrenfeld et al., 2016; Geider et al., 1996, 1998; Inomura et al.,
266 2020; Laws & Bannister, 1980; Talmy et al., 2013) analyses, the wintertime increase in transition
267 zone chlorophyll appears to be due to an increase in the chlorophyll to carbon ratio in response to
268 light-limited, nutrient-replete growth conditions. Extending this earlier work, we explicitly
269 resolve the latitudinal structure of photoacclimation dynamics at the basin scale and link the
270 decoupling of chlorophyll and carbon seasonality to the observed seasonality of latitudinal light
271 and nutrient supply.

272 This interpretation of TZCF chlorophyll dynamics extends previous studies investigating
273 transition zone seasonality (Ayers & Lozier, 2010; Bograd et al., 2004; Chai et al., 2003; Glover
274 et al., 1994; Le et al., 2019). These studies interpreted the southern extent of the wintertime
275 chlorophyll front as a phytoplankton carbon signal and sought the necessary environmental
276 drivers to explain elevated wintertime productivity. Our results, while supporting the existence of
277 a significant vertical wintertime nitrate flux (Chai et al., 2003; Glover et al., 1994), suggest that
278 wintertime nutrient supply has a limited impact on phytoplankton carbon and productivity.
279 Instead, wintertime nitrate supply relaxes nutrient stress, thus enriching the growth environment
280 to provide nutrients to fully acclimatize to light-limited conditions. Laboratory observations
281 show that nutrient stress decreases the chlorophyll to carbon ratio in light-lighted conditions by
282 diverting nitrogen from pigments and light-harvesting proteins (Geider et al., 1996; Inomura et
283 al., 2020; Laws & Bannister, 1980), supporting the suggestion that wintertime nutrient supplies
284 help maximize the seasonal photoacclimation response at transition zone latitudes. Established
285 empirical models also show a positive relationship between surface nitrate concentrations and the
286 N:C of particulate biomass (Galbraith & Martiny, 2015) which further suggest that
287 phytoplankton are able to build nitrogen rich pigments and light-harvesting proteins at high
288 nitrate supply.

289 This new perspective on seasonal chlorophyll dynamics in in the transition zone may motivate
290 re-analysis of higher trophic animal usage patterns in the region. Niche models for marine
291 mammals and seabirds have used satellite chlorophyll to represent bottom up drivers (Abrahms
292 et al., 2018; Block et al., 2011; Hazen et al., 2013). However, our results suggest that chlorophyll
293 serves as a poor proxy for transition zone phytoplankton carbon and that high chlorophyll levels
294 indicate a relatively low carbon content of cells, either through seasonal succession of low-light
295 adapted species or intra-specific acclimation. Because chlorophyll correlates strongly with sea
296 surface temperature (Bograd et al., 2004), periods of decorrelation between chlorophyll and
297 phytoplankton carbon, as characterized here, may provide the opportunity to isolate the roles of
298 temperature and food availability on animal habitat utilization.

299 *4.2 General implications for satellite observing of marine ecosystems*

300 This study reiterates the need to account for photoacclimation when interpreting the satellite
301 chlorophyll record, echoing calls from previous authors (Behrenfeld et al., 2005, 2016; Fox et al.,
302 2020; Graff et al., 2016; Omta et al., 2009). Although the dynamics and interannual trends in
303 chlorophyll have been insightful (Ayers & Lozier, 2010; Boyce et al., 2010, 2017; Glover et al.,
304 1994; Hammond et al., 2020), many studies continue to use chlorophyll as a proxy for
305 phytoplankton carbon and productivity. Complex relationships between chlorophyll, carbon, and

306 productivity, including the latitudinal dependence demonstrated here, complicate this
307 interpretation.

308 Beyond the North Pacific, our results suggest further work to elucidate the latitudinal structure of
309 light and nutrient supplies globally to better understand their role in coupling chlorophyll and
310 carbon dynamics. In the North Pacific, winter conditions conspire at the 30-40°N band to exhibit
311 deep winter mixing that drives a large seasonal cycle in light and nutrient supply which
312 maximizes seasonal photoacclimation; however, it is not clear whether the seasonal cycles of
313 light and nutrient supply in other basins will show similar latitudinal structure.

314 The relationship between mixed layer-averaged irradiance and Chl:C also has important
315 implications for observing climate impacts on marine ecosystems (Behrenfeld et al., 2016),
316 including multiple studies that have examined multidecadal trends in chlorophyll (Boyce et al.,
317 2010; Hammond et al., 2020; Henson et al., 2010). Warming of the upper water column has
318 increased stratification and reduced mixed layer depths in the North Pacific (Freeland, 2013) and
319 across the global ocean (Li et al., 2018), with trends expected to increase into the future (Fu et
320 al., 2016). These changes are often associated with reduced nutrient supply and productivity
321 (Behrenfeld et al., 2006; Fu et al., 2016), which are invoked to explain chlorophyll declines.
322 However, photoacclimation dynamics suggest that chlorophyll declines may also occur with
323 reduced mixed layers due to photoacclimation (higher light availability with mixed layer
324 shoaling) and may be uncorrelated or negatively correlated with changes in phytoplankton
325 carbon and productivity (Behrenfeld et al., 2016).

326 Going forward, we highlight the need to further integrate eco-physiology with satellite observing
327 of marine ecosystems to better understand the physiological growth conditions of phytoplankton
328 at large spatial scales. Continued progress has been made with carbon-based estimates of ocean
329 productivity that explicitly account for photoacclimation processes (Behrenfeld et al., 2005,
330 2016; Fox et al., 2020; Westberry et al., 2008). More recent work has further integrated resource-
331 allocation strategies into remote sensing models of phytoplankton growth (Tanioka et al., 2020)
332 which provide additional constraints on phytoplankton physiology by resolving cellular
333 stoichiometry as a function of light, nutrient supply, and temperature (Geider et al., 1998;
334 Inomura et al., 2020; Laws & Bannister, 1980).

335 **5 Conclusions**

336 In conclusion, our results suggest chlorophyll variability in the transition zone is primarily driven
337 by photoacclimation to nutrient replete, light-limited growth conditions found in the transition
338 zone winter. The latitudinal structure of seasonal light and nutrient supply creates conditions that
339 maximize seasonal photoacclimation and govern the TZCF chlorophyll signal. Further synthesis
340 of phytoplankton physiology and carbon-based remote-sensing of marine ecosystems will
341 improve our understanding of the phytoplankton growth environment and reduce uncertainties in
342 detecting climate change impacts on ocean ecosystems from space.

343 **Acknowledgments**

344 We acknowledge all the observational scientists and technologists that made this work possible.
345 GLB acknowledges funding from the Simons Foundations Postdoctoral Fellowship in Marine
346 Microbial Ecology. GLB, CP, GF, MJF acknowledge funding from the Simons Foundation

347 Collaboration on Computational Biogeochemical Modeling of Marine Ecosystems (CBIOMES)
348 and Simons Collaboration on Ocean Processes and Ecology (SCOPE). CP acknowledges funding
349 from the Undergraduate Research Opportunities Program at MIT. Data used in this study are
350 available publicly through <http://sites.science.oregonstate.edu/ocean.productivity/>,
351 <https://www.soda.umd.edu>, <http://mixedlayer.ucsd.edu/> and through the World Ocean Atlas
352 (Garcia et al., 2019). Details are given in the main text. All code to reproduce the analyses are
353 available publicly at https://github.com/gregbritten/transition_zone_chlorophyll

354 **References**

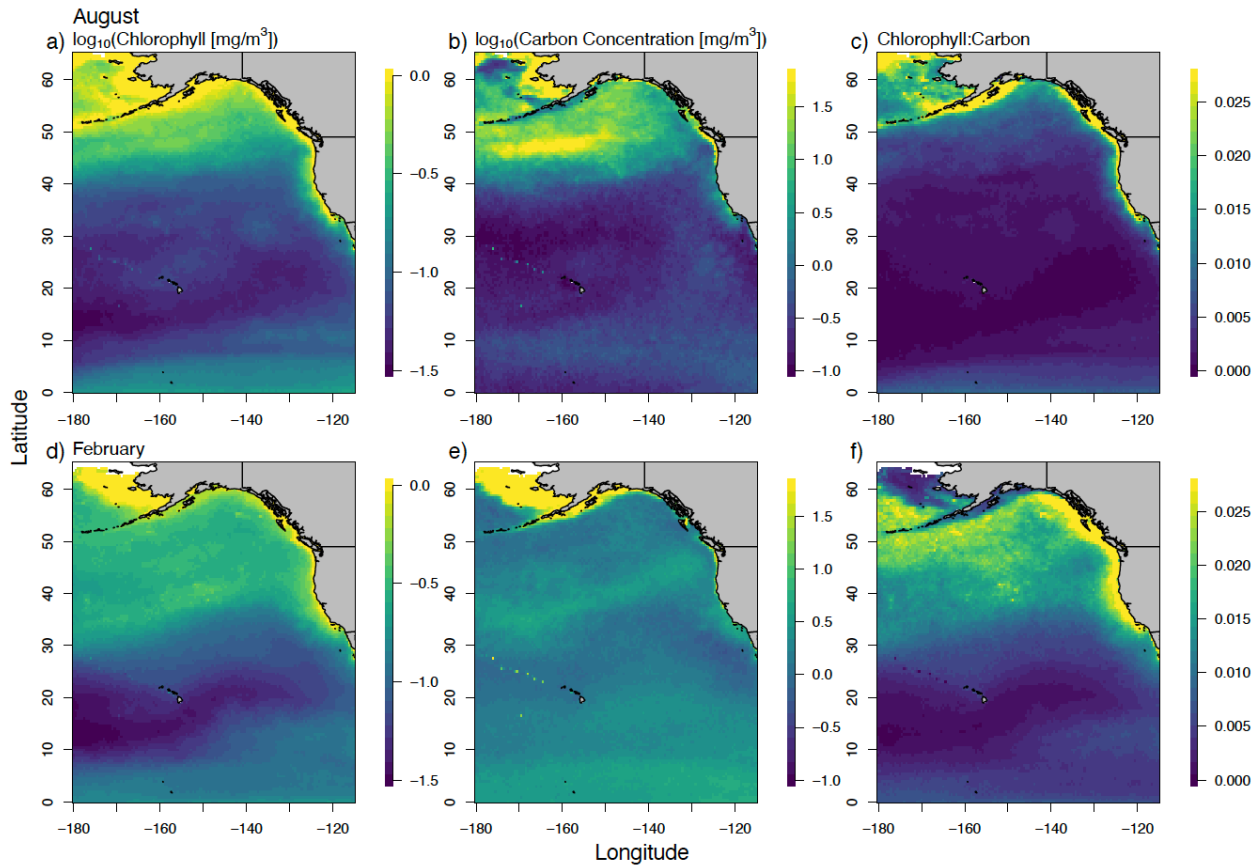
- 355 Abrahms, B., Hazen, E. L., Bograd, S. J., Brashares, J. S., Robinson, P. W., Scales, K. L., et al.
356 (2018). Climate mediates the success of migration strategies in a marine predator. *Ecology*
357 *Letters*, *21*(1), 63–71.
- 358 Ayers, J. M., & Lozier, M. S. (2010). Physical controls on the seasonal migration of the North
359 Pacific transition zone chlorophyll front. *Journal of Geophysical Research: Oceans*, *115*, 1–
360 11.
- 361 Behrenfeld, M. J., & Falkowski, P. G. (1997). Photosynthetic rates derived from satellite-based
362 chlorophyll concentration. *Limnology and Oceanography*, *42*(1), 1–20.
- 363 Behrenfeld, M. J., Boss, E., Siegel, D. A., & Shea, D. M. (2005). Carbon-based ocean
364 productivity and phytoplankton physiology from space. *Global Biogeochemical Cycles*,
365 *19*(1), 1–14.
- 366 Behrenfeld, M. J., O'Malley, R. T., Siegel, D. a, McClain, C. R., Sarmiento, J. L., Feldman, G.
367 C., et al. (2006). Climate-driven trends in contemporary ocean productivity. *Nature*,
368 *444*(7120), 752–725.
- 369 Behrenfeld, M. J., O'Malley, R. T., Boss, E. S., Westberry, T. K., Graff, J. R., Halsey, K. H., et
370 al. (2016). Revaluating ocean warming impacts on global phytoplankton. *Nature Climate*
371 *Change*, *6*(3), 323–330.
- 372 Block, B. A., Jonsen, I. D., Jorgensen, S. J., Winship, A. J., Shaffer, S. A., Bograd, S. J., et al.
373 (2011). Tracking apex marine predator movements in a dynamic ocean. *Nature*, *475*(7354),
374 86–90.
- 375 Bograd, S. J., Foley, D. G., Schwing, F. B., Wilson, C., Laurs, R. M., Polovina, J. J., et al.
376 (2004). On the seasonal and interannual migrations of the transition zone chlorophyll front.
377 *Geophysical Research Letters*, *31*(17), 1–5.
- 378 Boyce, D. G., Lewis, M. R., & Worm, B. (2010). Global phytoplankton decline over the past
379 century. *Nature*, *466*(7306), 591–6.
- 380 Boyce, D. G., Petrie, B., Frank, K. T., Worm, B., & Leggett, W. C. (2017). Environmental
381 structuring of marine plankton phenology. *Nature Ecology and Evolution*, *1*(10), 1484–
382 1494.

- 383 Chai, F., Jiang, M., Barber, R. T., Dugdale, R. C., & Chao, Y. (2003). Interdecadal variation of
384 the Transition Zone Chlorophyll Front: A physical-biological model simulation between
385 1960 and 1990. *Journal of Oceanography*, *59*(4), 461–475.
- 386 Evans, G. T., Parslow, J. S., Evans, G. T., & Parslow, J. S. (1985). A model of annual plankton
387 cycles. *Deep Sea Research Part B. Oceanographic Literature Review*, *32*(9), 759.
- 388 Follett, C. L., Dutkiewicz, S., Forget, G., Cael, B. B., & Follows, M. J. (2021). Moving
389 ecological and biogeochemical transitions across the North Pacific. *Limnology and*
390 *Oceanography*, *66*(6), 2442–2454.
- 391 Fox, J., Behrenfeld, M. J., Haëntjens, N., Chase, A., Kramer, S. J., Boss, E., et al. (2020).
392 Phytoplankton growth and productivity in the Western North Atlantic: Observations of
393 regional variability from the NAAMES field campaigns. *Frontiers in Marine Science*,
394 *7*(24), 1–15.
- 395 Freeland, H. J. (2013). Evidence of change in the winter mixed layer in the Northeast Pacific
396 Ocean: A problem revisited. *Atmosphere-Ocean*, *51*, 126–133.
- 397 Fu, W., Randerson, J. T., & Moore, J. K. (2016). Climate change impacts on net primary
398 production (NPP) and export production (EP) regulated by increasing stratification and
399 phytoplankton community structure in the CMIP5 models. *Biogeosciences*, *13*, 5151–5170.
- 400 Galbraith, E. D., & Martiny, A. C. (2015). A simple nutrient-dependence mechanism for
401 predicting the stoichiometry of marine ecosystems. *Proceedings of the National Academy of*
402 *Sciences*, *112*(27), 8199–8204.
- 403 Garcia, H. E., Boyer, T. P., Baranova, O. K., Locarnini, R. A., Mishonov, A. V., Grodsky, A., et
404 al. (2019). World Ocean Atlas 2018. *Product Documentation*, *1*, 1–20.
- 405 Geider, R. J., Osborne, B. A., & Raven, J. A. (1986). Growth, photosynthesis, and maintenance
406 metabolic cost in the diatom *Phaeodactylum tricornutum* at very low light levels. *Journal of*
407 *Phycology*, *22*, 39–48.
- 408 Geider, R. J., MacIntyre, H. L., & Kana, T. M. (1996). A dynamic model of photoadaptation in
409 phytoplankton. *Limnology and Oceanography*, *41*(1), 1–15.
- 410 Geider, R. J., MacIntyre, H. L., & Kana, T. M. (1998). A dynamic regulatory model of
411 phytoplanktonic acclimation to light, nutrients, and temperature. *Limnology and*
412 *Oceanography*, *43*(4), 679–694.
- 413 Glover, M., Wroblewski, J. S., & McClain, C. R. (1994). Dynamics of the transition zone in
414 coastal zone color scanner-sensed ocean color in the North Pacific during oceanographic
415 spring. *Journal of Geophysical Research*, *99*, 7501–7511.
- 416 Graff, J. R., Westberry, T. K., Milligan, A. J., Brown, M. B., Dall’Olmo, G., Reifel, K. M., &
417 Behrenfeld, M. J. (2016). Photoacclimation of natural phytoplankton communities. *Marine*
418 *Ecology Progress Series*, *542*, 51–62.

- 419 Hammond, M. L., Beaulieu, C., Henson, S. A., & Sahu, S. K. (2020). Regional surface
420 chlorophyll trends and uncertainties in the global ocean. *Scientific Reports*, *10*(1), 1–9.
- 421 Hazen, E. L., Jorgensen, S., Rykaczewski, R. R., Bograd, S. J., Foley, D. G., Jonsen, I. D., et al.
422 (2013). Predicted habitat shifts of Pacific top predators in a changing climate. *Nature*
423 *Climate Change*, *3*(3), 234–238.
- 424 Henson, S. A., Sarmiento, J. L., Dunne, J. P., Bopp, L., Lima, I., Doney, S. C., et al. (2010).
425 Detection of anthropogenic climate change in satellite records of ocean chlorophyll and
426 productivity. *Biogeosciences*, *7*(2), 621–640.
- 427 Holte, J., Talley, L. D., Gilson, J., & Roemmich, D. (2017). An Argo mixed layer climatology
428 and database. *Geophysical Research Letters*, *44*(11), 5618–5626.
- 429 Inomura, K., Omta, A. W., Talmy, D., Bragg, J., Deutsch, C., & Follows, M. J. (2020). A
430 mechanistic model of macromolecular allocation, elemental stoichiometry, and growth rate
431 in phytoplankton. *Frontiers in Microbiology*, *11*, 1–9.
- 432 Jackson, T., Sathyendranath, S., & Platt, T. (2017). An exact solution for modeling
433 photoacclimation of the carbon-to-chlorophyll ratio in phytoplankton. *Frontiers in Marine*
434 *Science*, *4*, 1–10.
- 435 Kappes, M. A., Shaffer, S. A., Tremblay, Y., Foley, D. G., Palacios, D. M., Robinson, P. W., et
436 al. (2010). Hawaiian albatrosses track interannual variability of marine habitats in the North
437 Pacific. *Progress in Oceanography*, *86*(2), 246–260.
- 438 Laws, E. A., & Bannister, T. T. (1980). Nutrient- and light-limited growth of *Thalassiosira*
439 *fluviatilis* in continuous culture with implications for phytoplankton growth in the ocean.
440 *Limnology and Oceanography*, *25*, 457–473.
- 441 Le, C., Wu, S., Hu, C., Beck, M. W., & Yang, X. (2019). Phytoplankton decline in the eastern
442 North Pacific transition zone associated with atmospheric blocking. *Global Change*
443 *Biology*, *25*(10), 3485–3493.
- 444 Li, G., Cheng, L., Zhu, J., Trenberth, K. E., Mann, M. E., & Abraham, J. P. (2018). Increasing
445 ocean stratification over the past half-century. *Nature Climate Change*, (12), 1116–1123.
- 446 Maritorena, S., Siegel, D. A., & Peterson, A. R. (2002). Optimization of a semianalytical ocean
447 color model for global-scale applications. *Applied Optics*, *41*(15), 2705.
- 448 Omta, A. W., Llido, J., Garçon, V., Kooijman, S. A. L. M., & Dijkstra, H. A. (2009). The
449 interpretation of satellite chlorophyll observations: The case of the Mozambique Channel.
450 *Deep-Sea Research Part I: Oceanographic Research Papers*, *56*(6), 974–988.
- 451 Polovina, J. J., Howell, E., Kobayashi, D. R., & Seki, M. P. (2001). The transition zone
452 chlorophyll front, a dynamic global feature defining migration and forage habitat for marine
453 resources. *Progress in Oceanography*, *49*, 469–483.

- 454 Polovina, J. J., Howell, E. A., Kobayashi, D. R., & Seki, M. P. (2017). The Transition Zone
 455 Chlorophyll Front updated: Advances from a decade of research. *Progress in*
 456 *Oceanography*, 150, 79–85.
- 457 Sathyendranath, S., Platt, T., Kovač, Ž., Dingle, J., Jackson, T., Brewin, R. J. W., et al. (2020).
 458 Reconciling models of primary production and photoacclimation. *Applied Optics*, 59(10),
 459 100–114.
- 460 Silsbe, G., Behrenfeld, M., Halsey, K., Milligan, A., & Westberry, T. (2016). The CAFE model:
 461 A net production model for global ocean phytoplankton. *Global Biogeochemical Cycles*, 30,
 462 1756–1777.
- 463 Son, S. H., & Wang, M. (2015). Diffuse attenuation coefficient of the photosynthetically
 464 available radiation Kd(PAR) for global open ocean and coastal waters. *Remote Sensing of*
 465 *Environment*, 159, 250–258.
- 466 Talmy, D., Blackford, J., Hardman-Mountford, N. J., Dumbrell, A. J., & Geider, R. J. (2013). An
 467 optimality model of photoadaptation in contrasting aquatic light regimes. *Limnology and*
 468 *Oceanography*, 58(5), 1802–1818.
- 469 Tanioka, T., Fichot, C. G., & Matsumoto, K. (2020). Toward determining the spatio-temporal
 470 variability of upper-ocean ecosystem stoichiometry from satellite remote sensing. *Frontiers*
 471 *in Marine Science*, 7, 1–16.
- 472 Venables, H., & Moore, C. M. (2010). Phytoplankton and light limitation in the Southern Ocean:
 473 Learning from high-nutrient, high-chlorophyll areas. *Journal of Geophysical Research*, 115,
 474 1–12.
- 475 Werdell, P. J., Franz, B. A., Bailey, S. W., Feldman, G. C., Boss, E., Brando, V. E., et al. (2013).
 476 Generalized ocean color inversion model for retrieving marine inherent optical properties.
 477 *Applied Optics*, 52, 2019–2037.
- 478 Westberry, T., Behrenfeld, M. J., Siegel, D. A., & Boss, E. (2008). Carbon-based primary
 479 productivity modeling with vertically resolved photoacclimation. *Global Biogeochemical*
 480 *Cycles*, 22(2), 1–18.
- 481 Xu, Y., Nieto, K., Teo, S. L. H., McClatchie, S., & Holmes, J. (2017). Influence of fronts on the
 482 spatial distribution of albacore tuna (*Thunnus alalunga*) in the Northeast Pacific over the
 483 past 30 years (1982–2011). *Progress in Oceanography*, 150, 72–78.

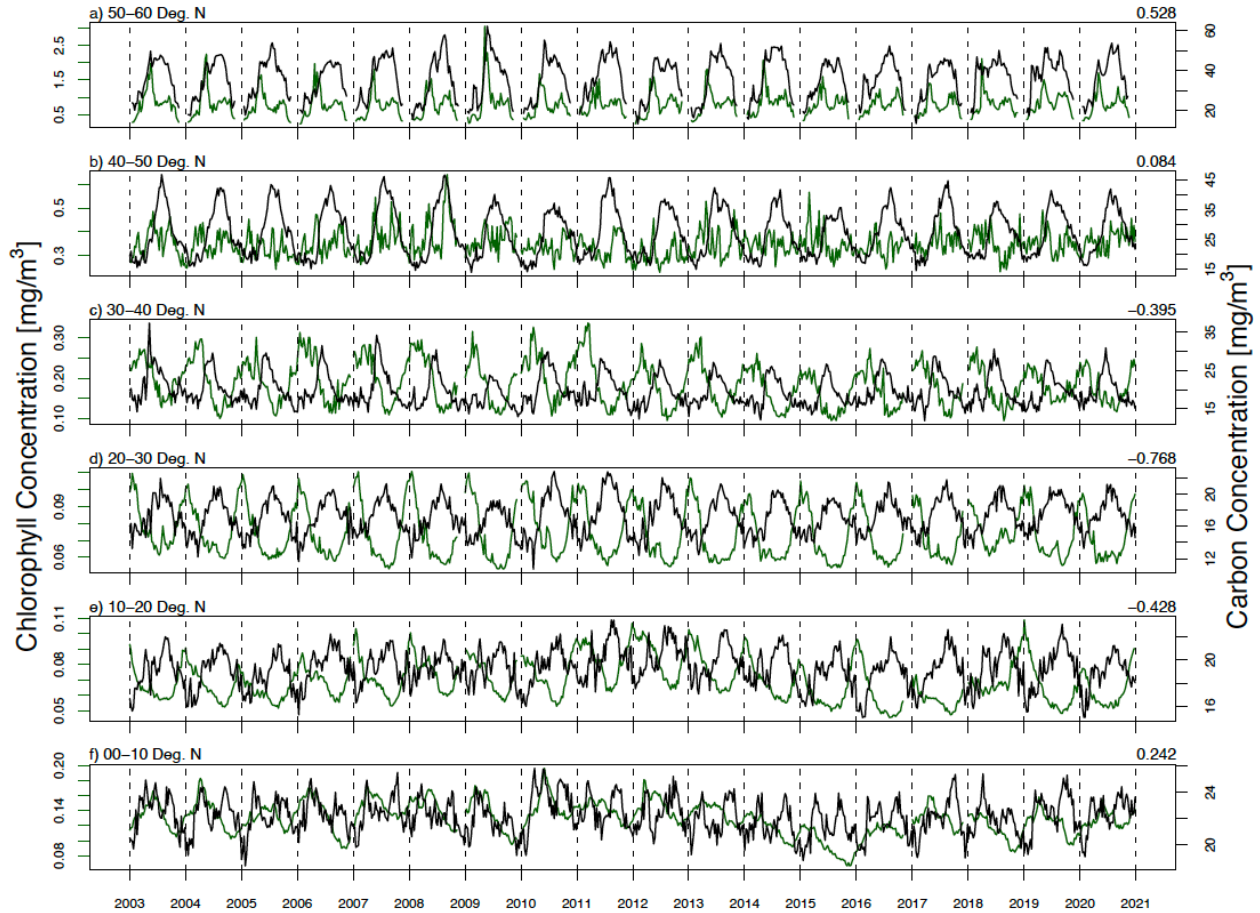
485



486

487 **Figure 1. Satellite-estimated climatology for surface chlorophyll concentrations, carbon**
 488 **concentrations, and their ratio for the months of August and February in the Northeast**
 489 **Pacific.** Panels a-c give the climatological chlorophyll, carbon, and chlorophyll:carbon ratio
 490 distributions for August, respectively. Panels d-f give the same respective fields for February.
 491

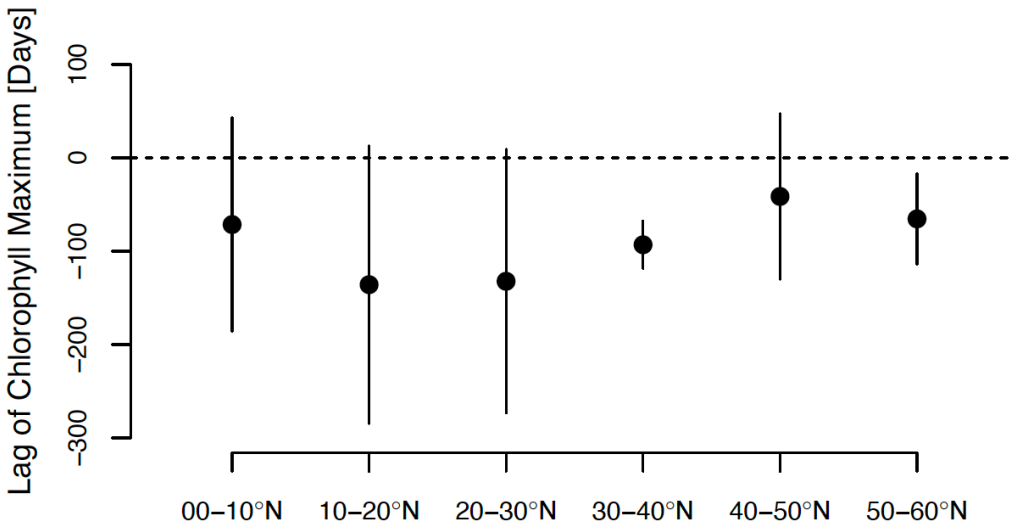
492



493

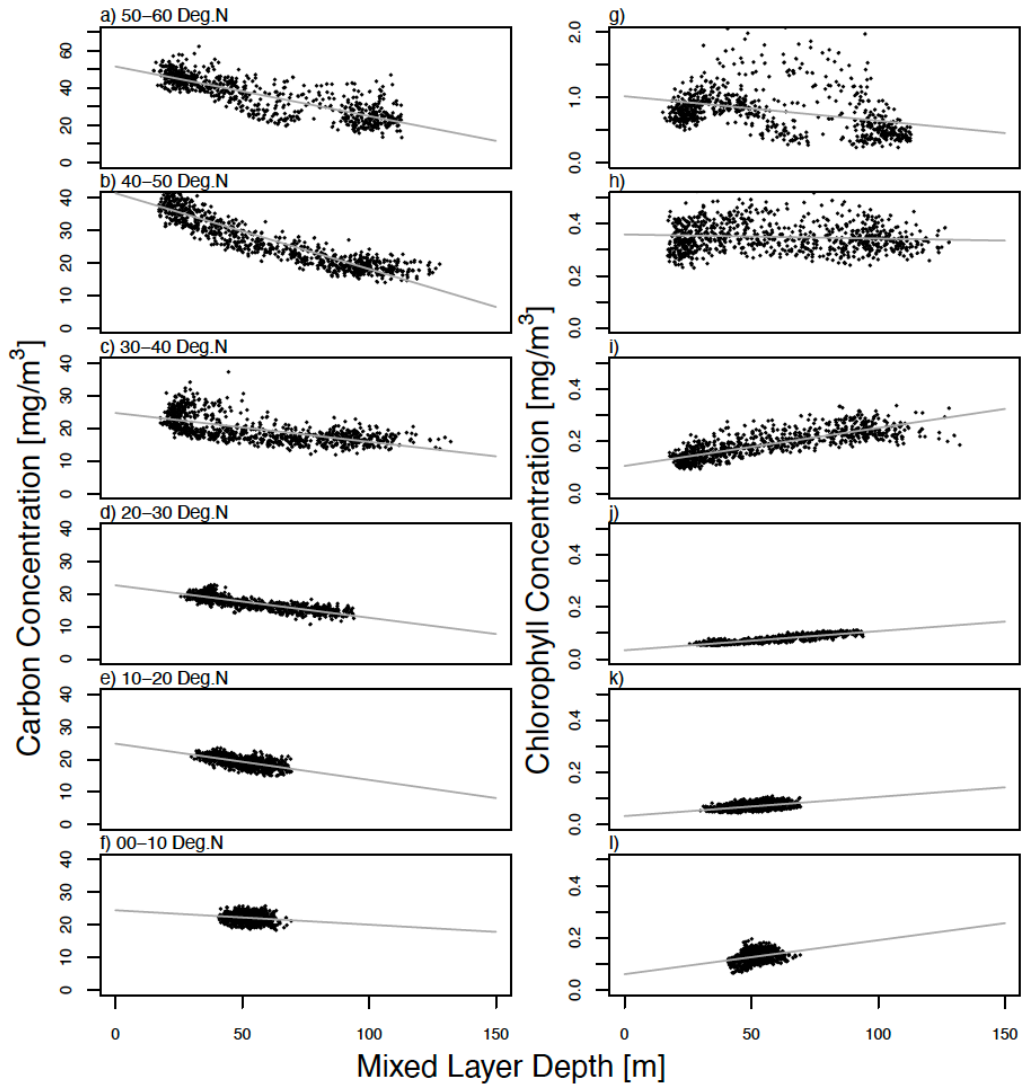
494 **Figure 2. Latitudinal time series of chlorophyll and carbon concentrations.** Chlorophyll is
 495 given with green lines and carbon is given with black. Rows represent different latitude bands.
 496 Latitudinal range is given in the top left of each panel. Correlation coefficient between the two
 497 series is given in the top right of each panel. Vertical dashed lines show January 01 of each year.
 498 Note the differing axis limits across panels.

499
500



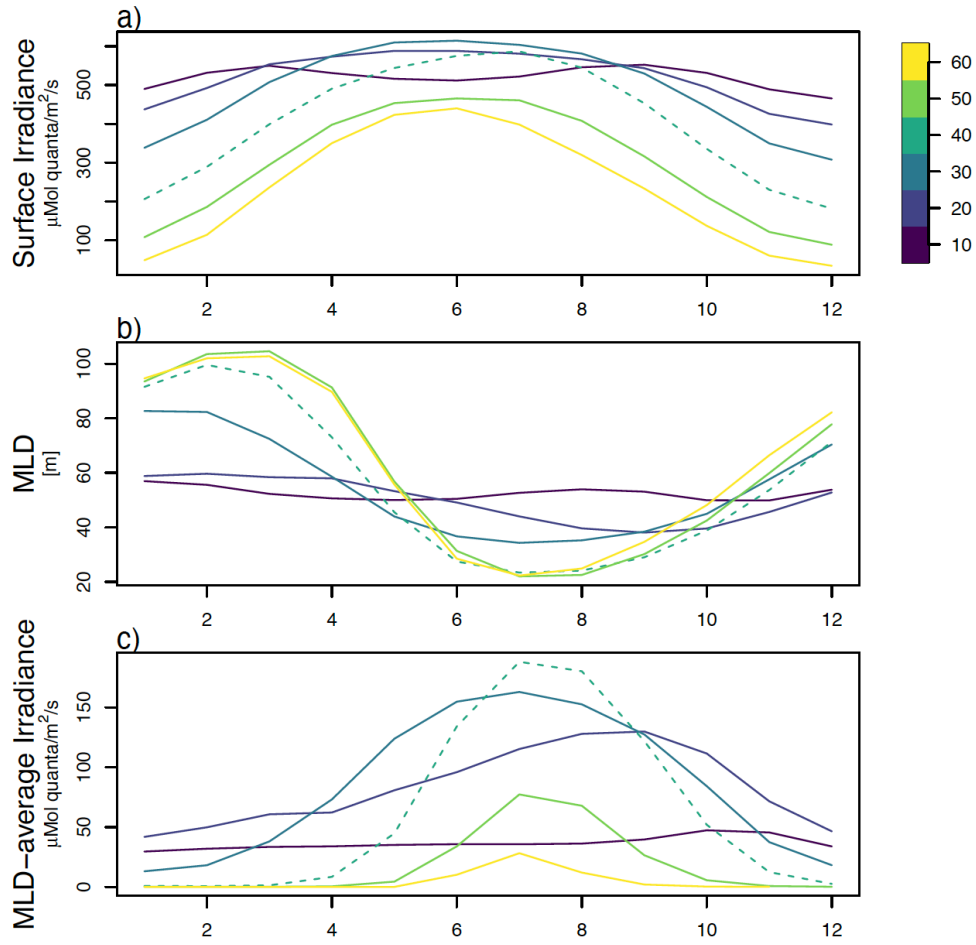
501
502

503 **Figure 3. Means and standard deviations of the lag between seasonal chlorophyll and**
 504 **carbon maxima.** Maxima are taken within individual years according to latitudinal time series in
 505 Figure 2. Mean and standard deviations are calculated across years. Negative values indicate that
 506 chlorophyll peaks before carbon in the seasonal cycle.



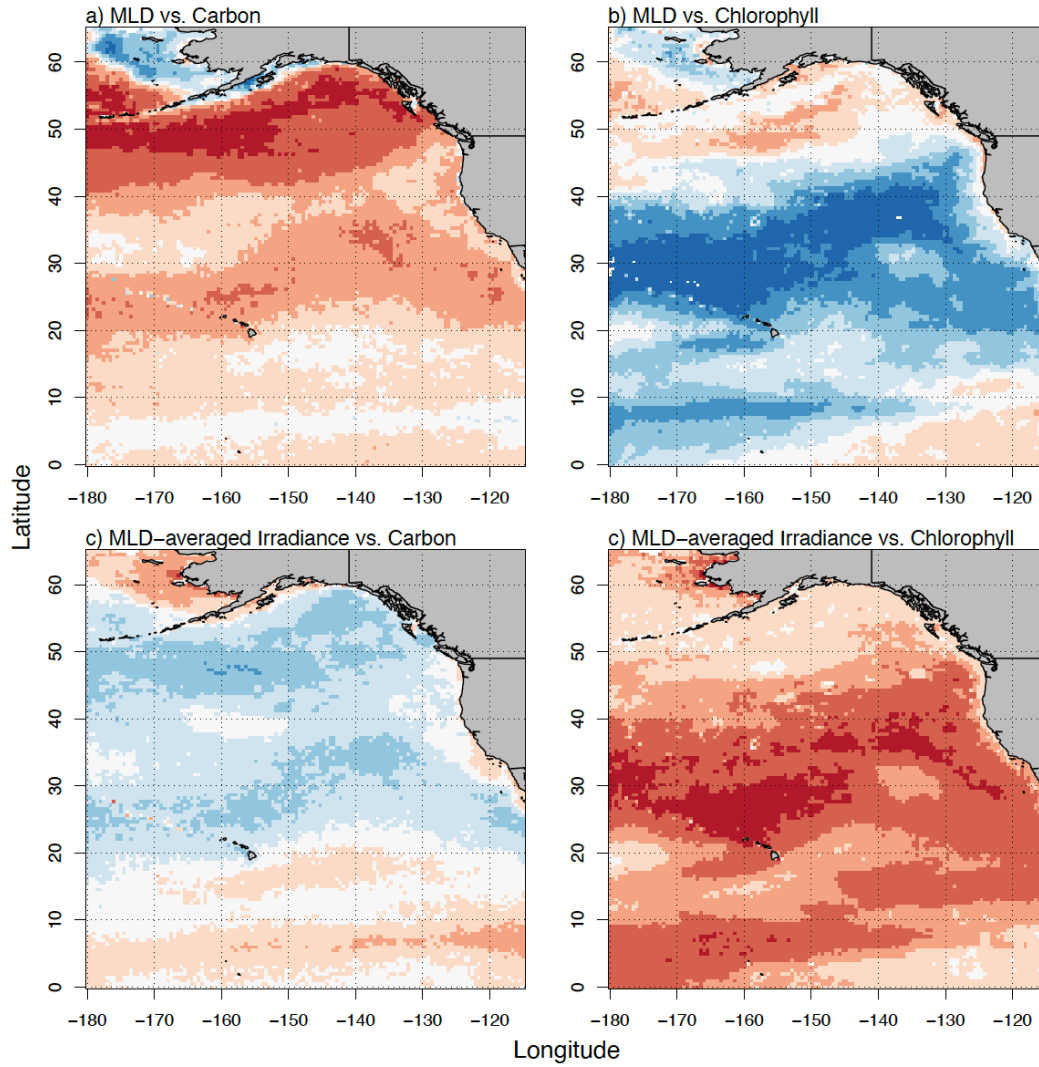
507

508 **Figure 4. Latitudinal relationships between carbon and chlorophyll concentrations with**
 509 **respect to mixed layer depth.** Left column (panels a-f) gives the relationships between carbon
 510 and mixed layer depth. Right column (panels g-l) gives the relationships with chlorophyll. Rows
 511 are latitude bands as in Figure 2. Latitude range is given in the top left of left column panels.
 512 Grey lines give the ordinary least squares regression line.



513
514
515
516
517
518
519

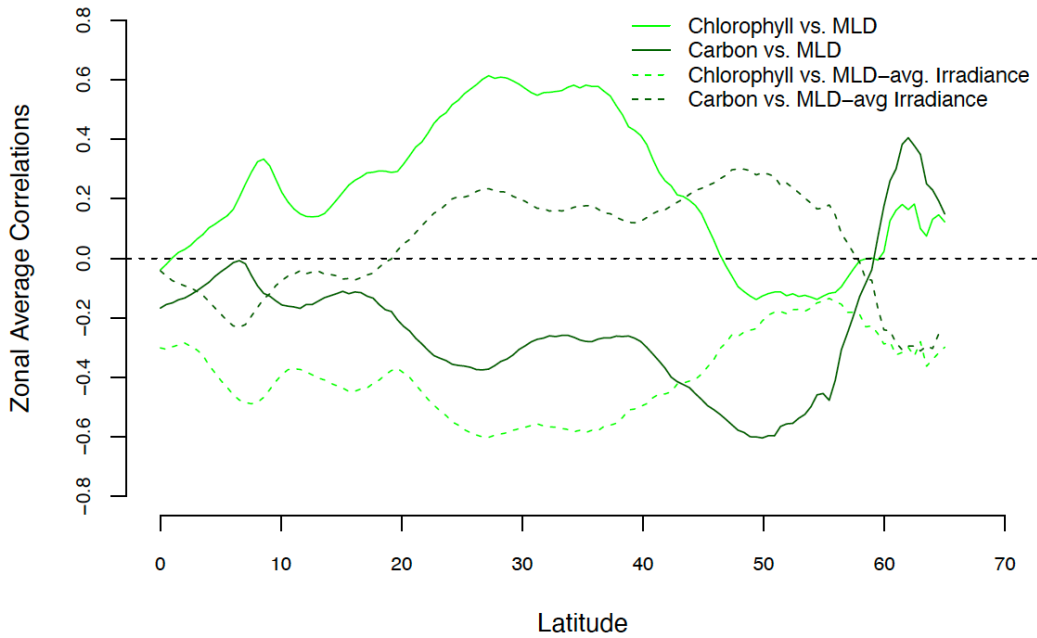
Figure 5. Seasonal climatology of day-averaged surface irradiance (a), mixed layer depth (b), and day-averaged mixed layer-averaged irradiance (c) for ten-degree latitude bands in the Northeast Pacific. Color bar gives the latitude bands for each line. Dashed line indicates the transition zone (30-40°N).



520
521

522 **Figure 6. Time series correlation coefficients between mixed layer depth (MLD) vs. carbon**
 523 **concentration (a), MLD vs. chlorophyll concentration (b), MLD-averaged irradiance vs.**
 524 **carbon concentration (c), and MLD-averaged irradiance vs. chlorophyll concentration (d).**
 525 **Correlations are calculated at each grid cell using the 20-year satellite time series record.**

526



527

528

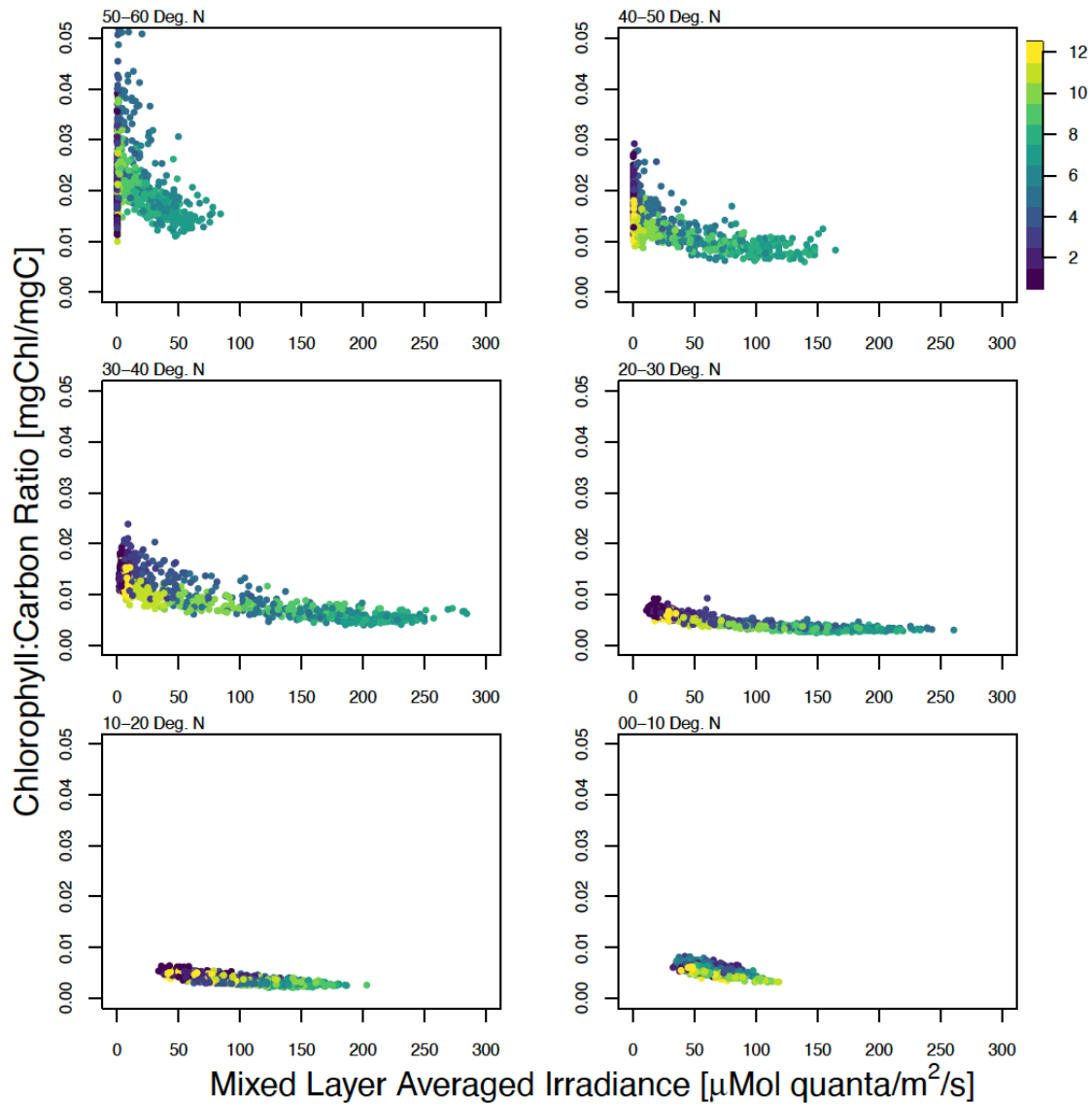
529

530

531

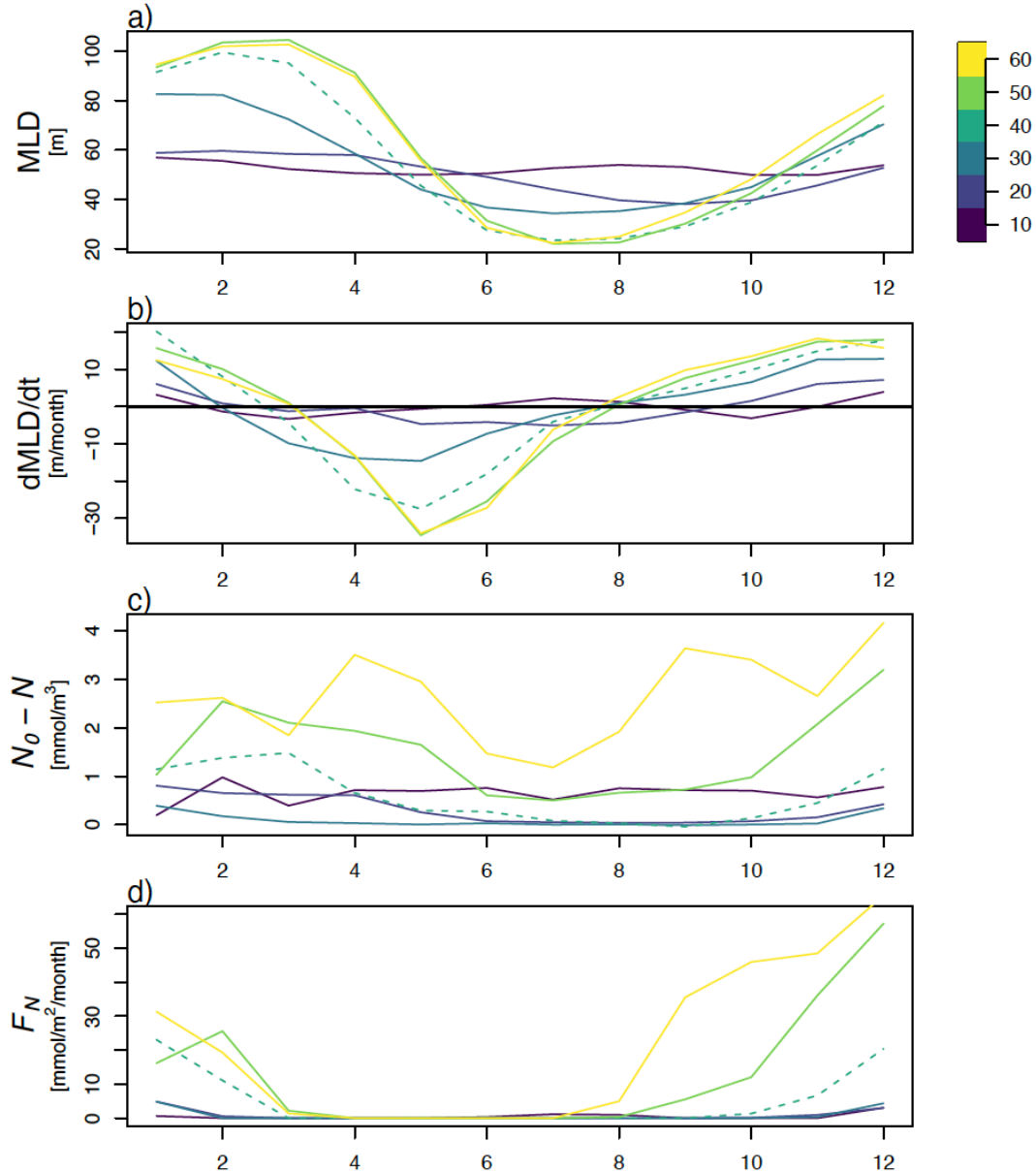
532

Figure 7. Zonally averaged correlations of the maps presented in Figure 6. Chlorophyll vs. mixed layer depth (MLD) and chlorophyll vs. MLD-averaged irradiance are given in solid and dashed light green lines, respectively. Carbon vs. mixed layer depth (MLD) and carbon vs. MLD-averaged irradiance are given in solid and dashed dark green lines, respectively. Black horizontal dashed line gives the zero-correlation line.



533

534 **Figure 8. Relationships between mixed layer-averaged irradiance and the satellite-**
 535 **estimated chlorophyll:carbon ratio.** Each box represents a ten-degree latitude band with the
 536 limits given in the upper left of each panel. Color represents month.
 537



538
539
540
541
542
543

Figure 9. Climatological seasonal nitrate entrainment flux across latitudes. Colors represent ten-degree latitude bands as in Figure 5. Panel a gives the climatological seasonal cycle in mixed layer depth. Panel b gives the entrainment velocity (solid black gives the zero line). Panel c gives the nitrate gradient evaluated between the mixed layer and one meter below. Panel d gives the calculated entrainment flux. Dashed lines represent the transition zone (30-40°N).

SUPPLEMENTAL INFORMATION

Seasonal photoacclimation in the North Pacific Transition Zone

Gregory L. Britten¹, Christine Padalino^{1,2}, Gaël Forget¹, Michael J. Follows¹

¹Program in Atmospheres, Oceans, and Climate, Massachusetts Institute of Technology

²Department of Chemical Engineering, Massachusetts Institute of Technology

Corresponding author: Gregory L. Britten (gbritten@mit.edu)

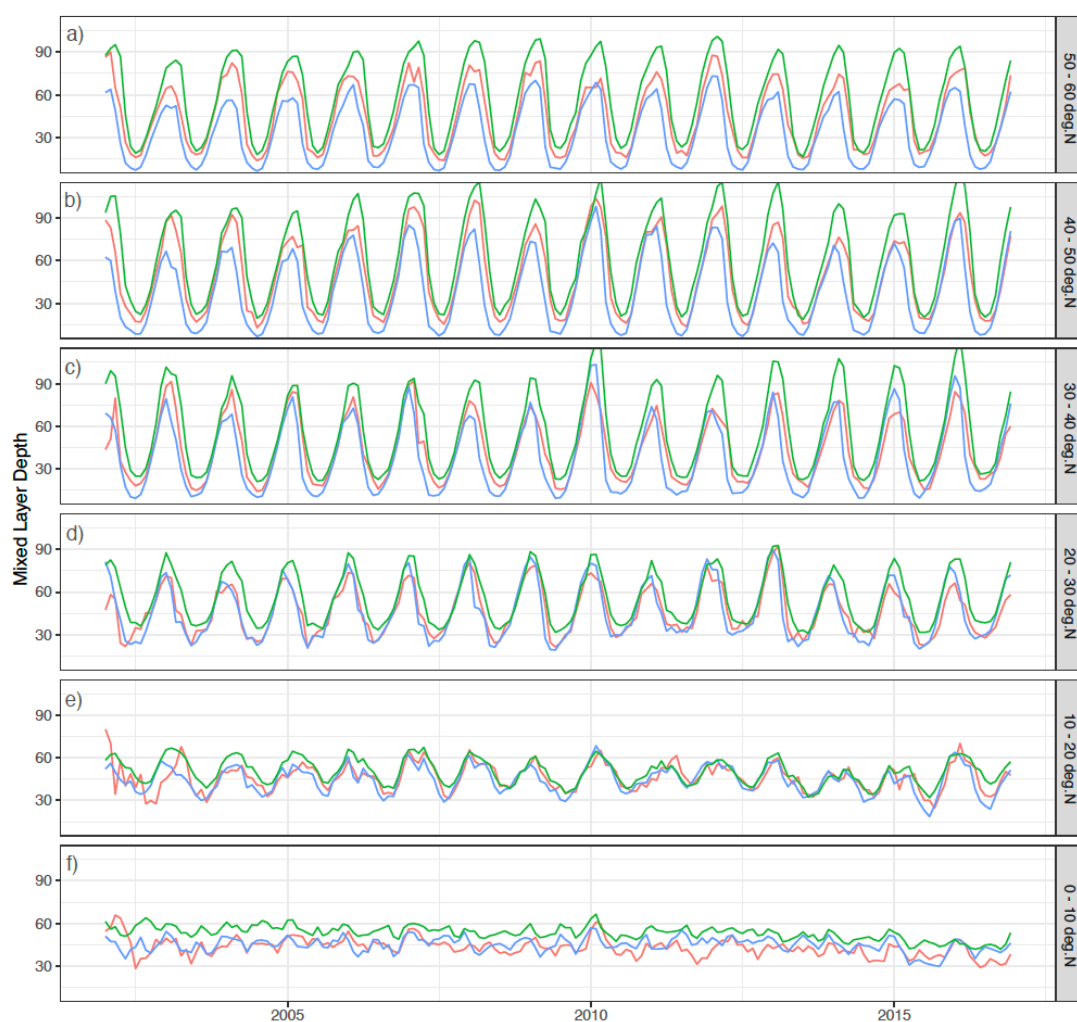


Figure S1. Time series of the three mixed layer estimates considered in this study. Each panel corresponds to a ten-degree latitude band (labels on the right of each panel). Argo observations are given in red, HyCOM reanalysis is in green, SODA reanalysis is in blue. We note small deviations in the amplitude across mixed layer estimates but no appreciable deviation in phasing which controls the correlations analyzed in the paper.

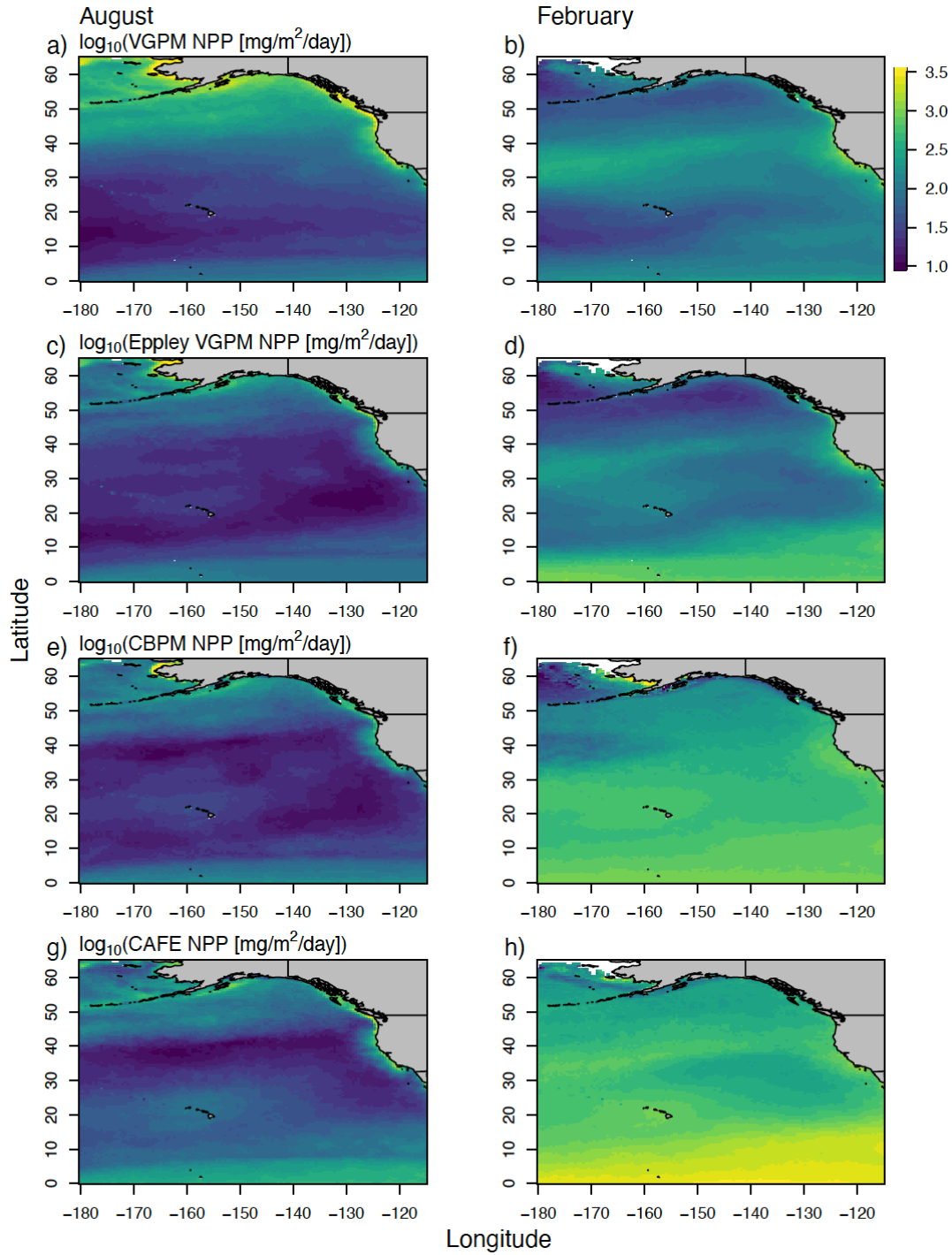


Figure S2. Comparison of August (left column) and February (right column) net primary productivity according to four different satellite based net primary productivity models. Model acronym is given in left column panel labels. See main text for details.

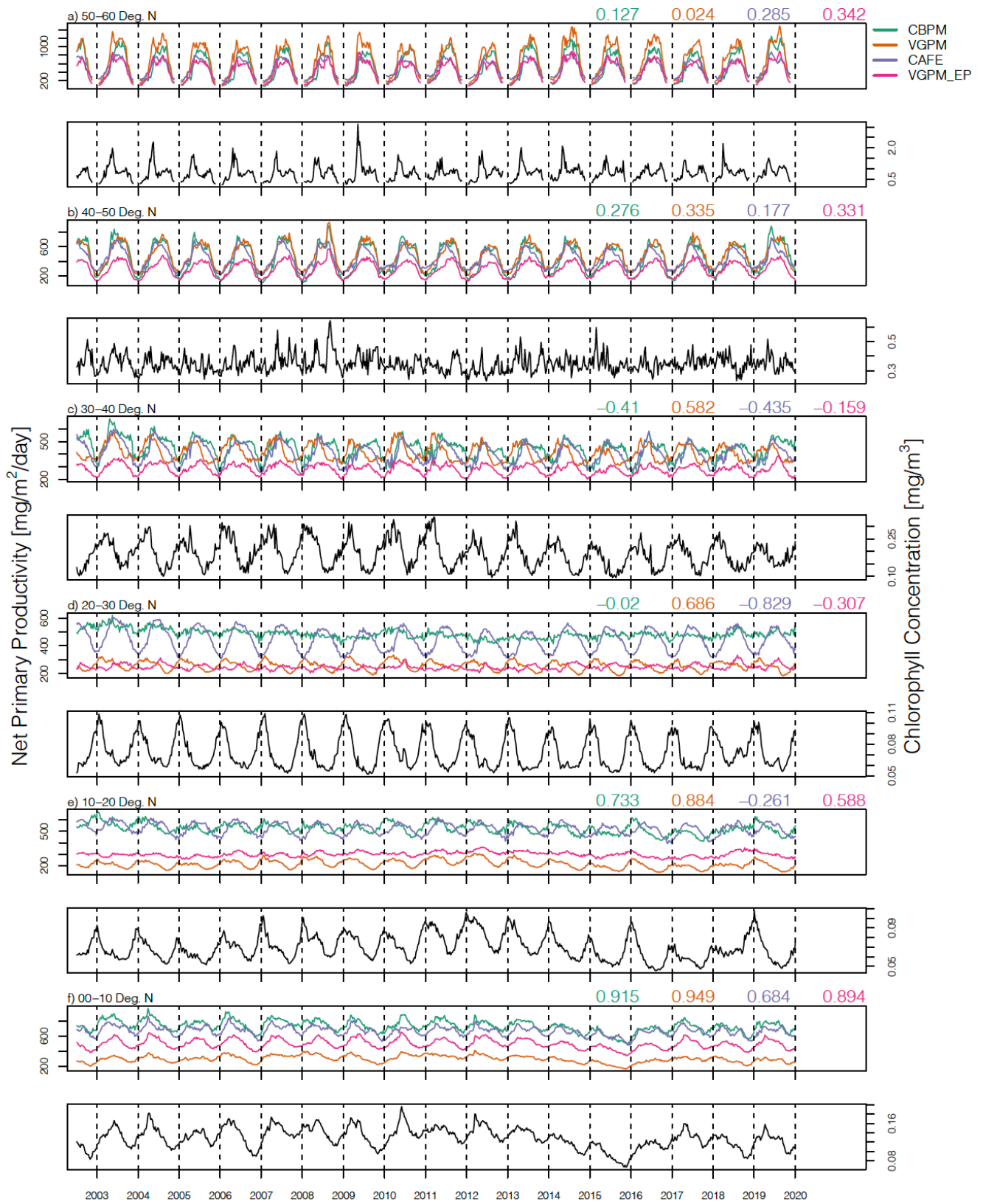


Figure S3. Time series and interannual correlations between four net primary productivity models and chlorophyll. Each pair of panels gives time series for a ten-degree latitude band (labeled in the top left). Net primary productivity models are colored. Carbon-based productivity model (CBPM) is green; vertically generalized productivity model (VGPM) is orange; carbon, assimilation, and fluorescence-resolving model (CAFÉ) is blue; vertically generalized productivity model with the Eppley temperature dependence (VGPM_EP) is in red. The chlorophyll time series corresponding to each latitude band is given in black under each net primary productivity panel. Colored numbers give the correlation coefficient between each net primary productivity model and chlorophyll.

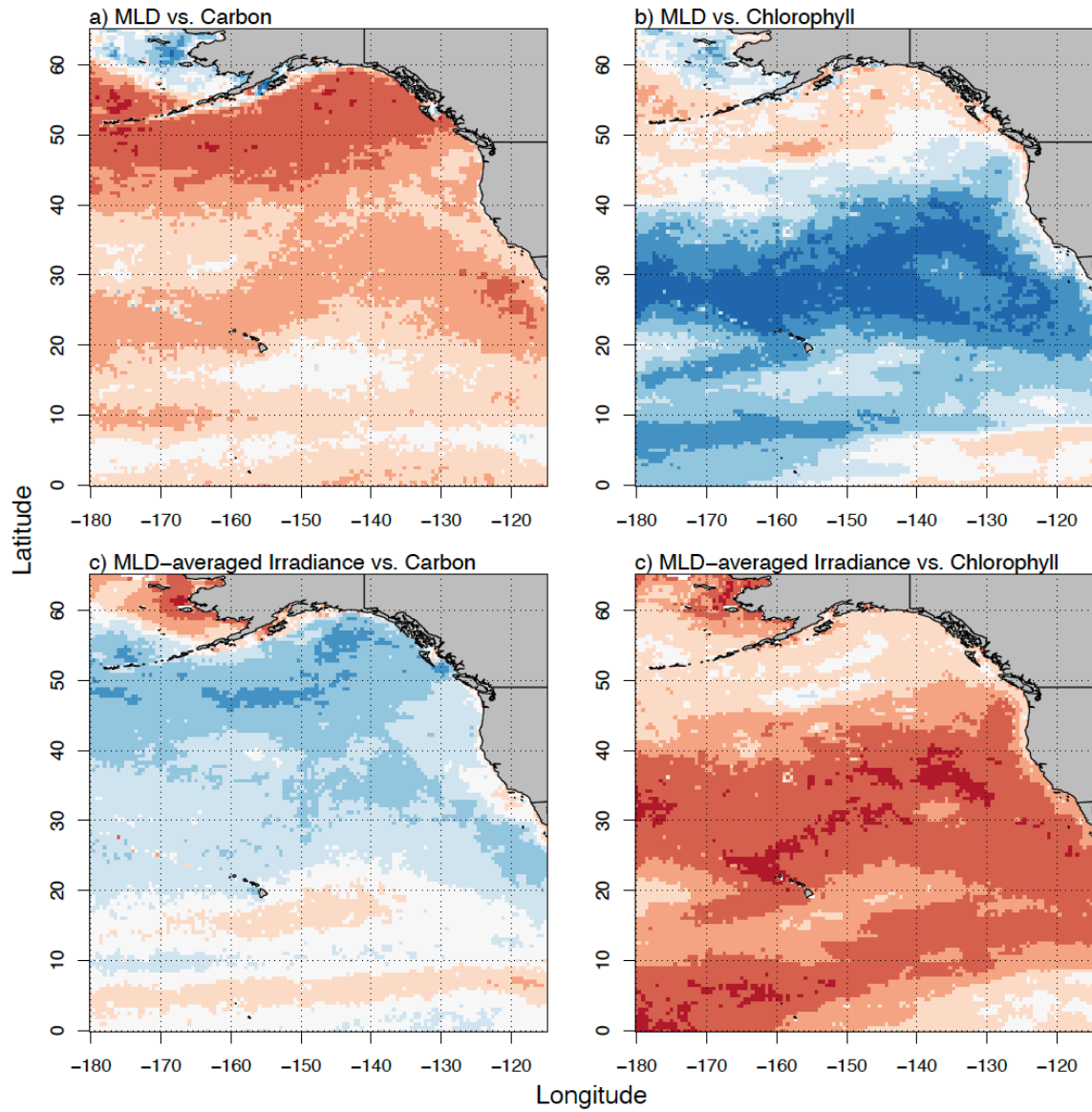


Figure S4. As in Figure 6 of the main text but using mixed layer depth estimates from the Simple Ocean Data Assimilation (SODA) reanalysis product. See main text for details.

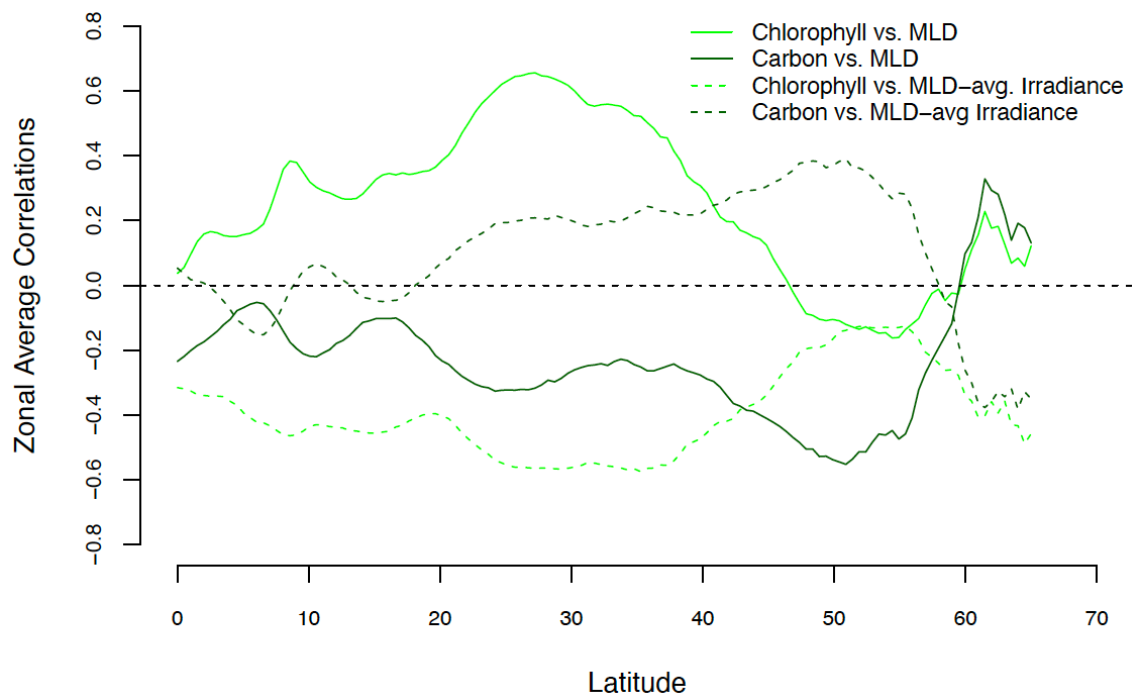


Figure S5. As in Figure 7 of the main text but using mixed layer depth estimates from the Simple Ocean Data Assimilation (SODA) mixed layer depth reanalysis product. See main text for details.

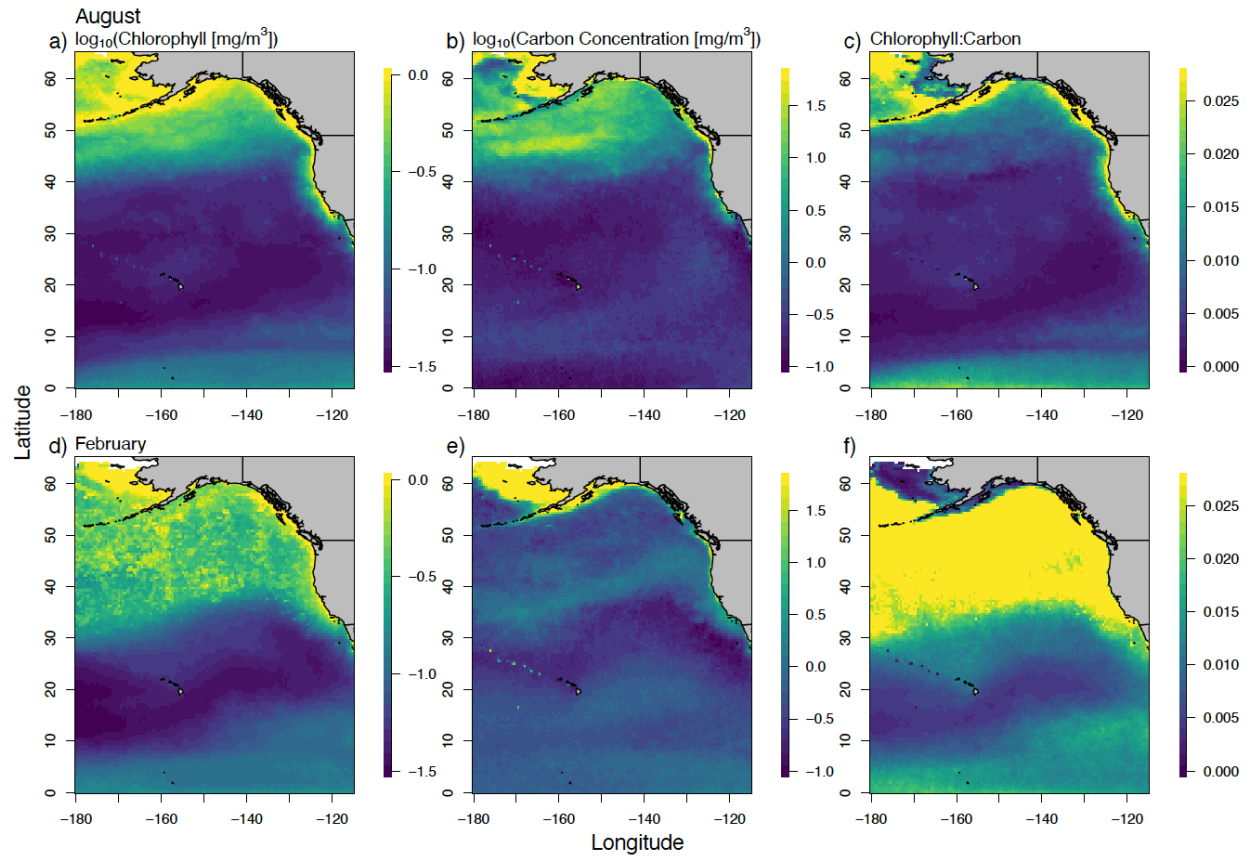


Figure S6. As in Figure 1 of the main text but using chlorophyll concentrations and backscatter coefficients estimated from the Garver-Siegel-Maritorena (GSM) ocean color inversion algorithm (Maritorena et al., 2002). Backscatter coefficients are converted to phytoplankton carbon estimates using the equations given in Behrenfeld et al., (2005) and Westberry et al., (2008).

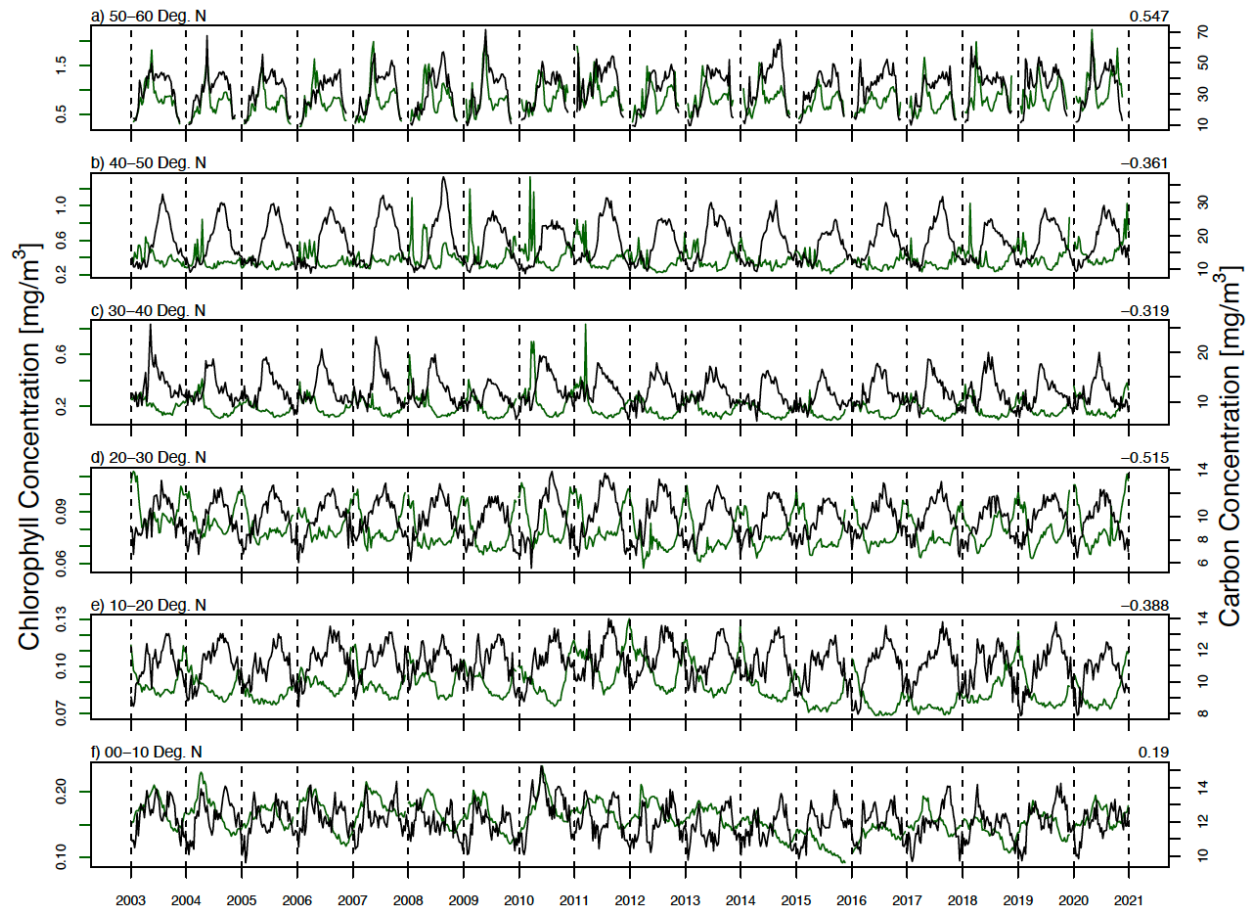


Figure S7. As in Figure 2 of the main text but using chlorophyll concentrations and backscatter coefficients estimated from the Garver-Siegel-Maritorena (GSM) ocean color inversion algorithm (Maritorena et al., 2002).

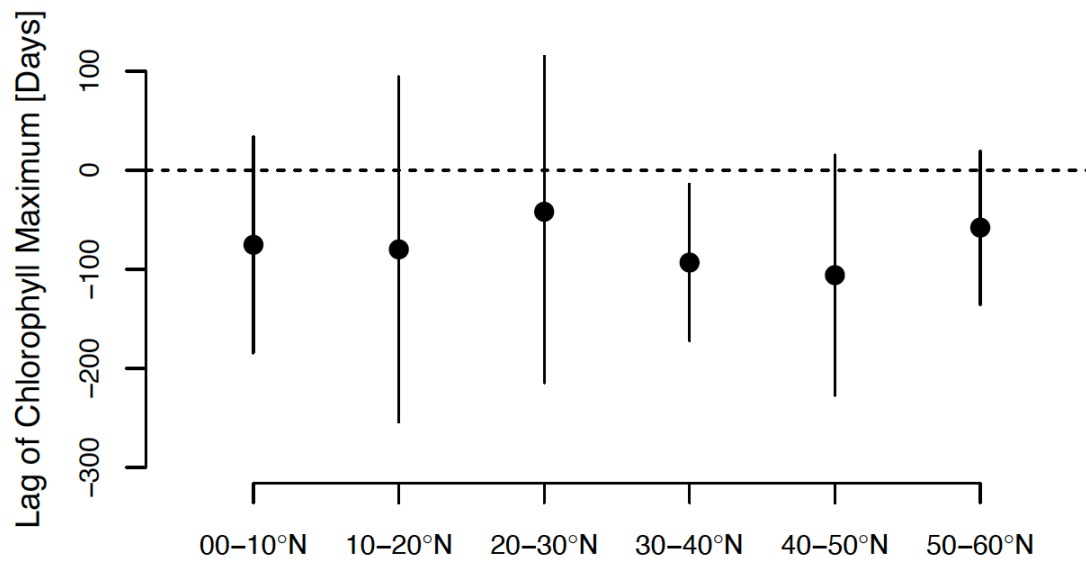


Figure S8. As in Figure 3 of the main text but using chlorophyll concentrations and backscatter coefficients estimated from the Garver-Siegel-Maritorena (GSM) ocean color inversion algorithm (Maritorena et al., 2002).

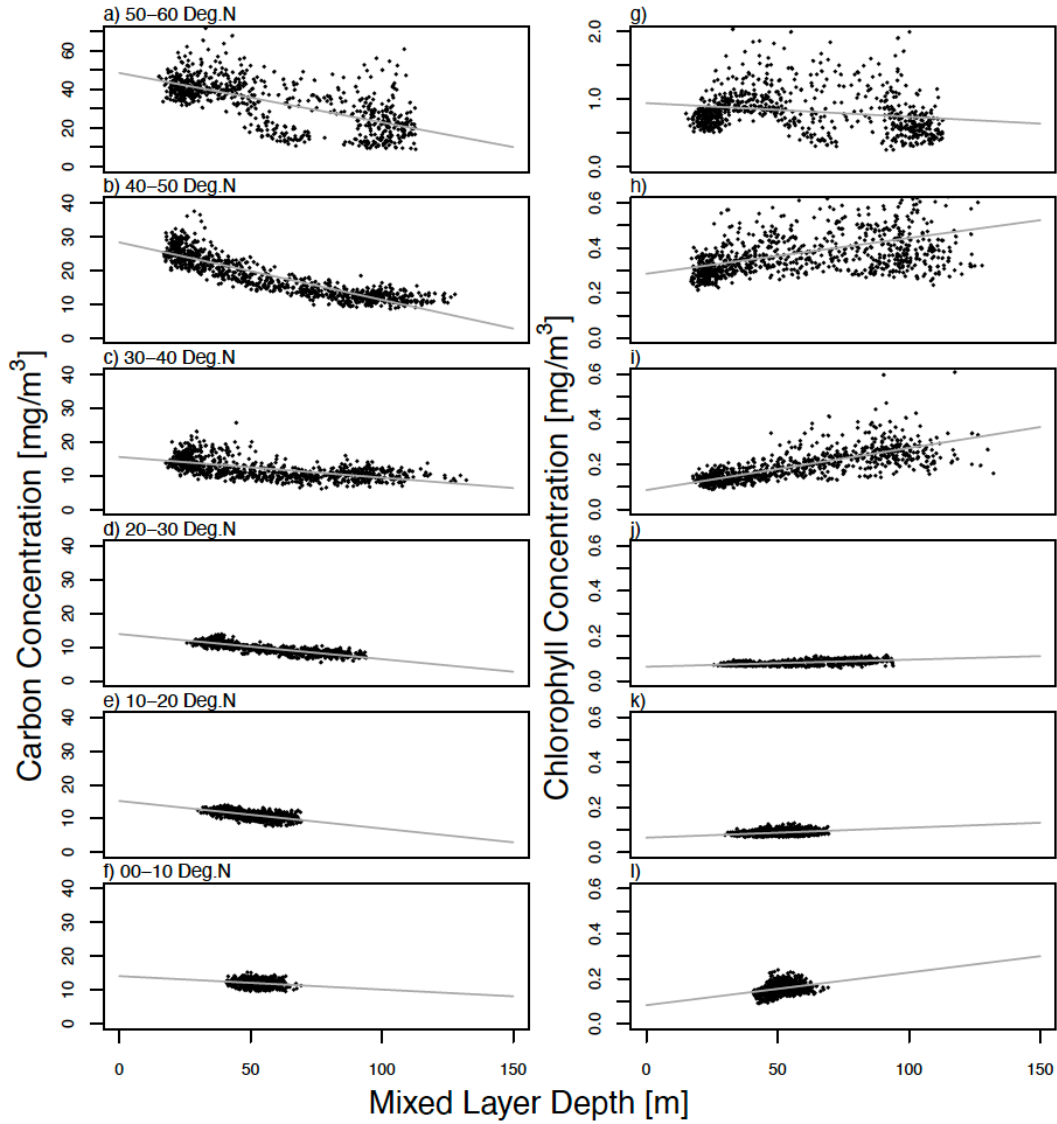


Figure S9. As in Figure 4 of the main text but using chlorophyll concentrations and backscatter coefficients estimated from the Garver-Siegel-Maritorena (GSM) ocean color inversion algorithm (Maritorena et al., 2002).

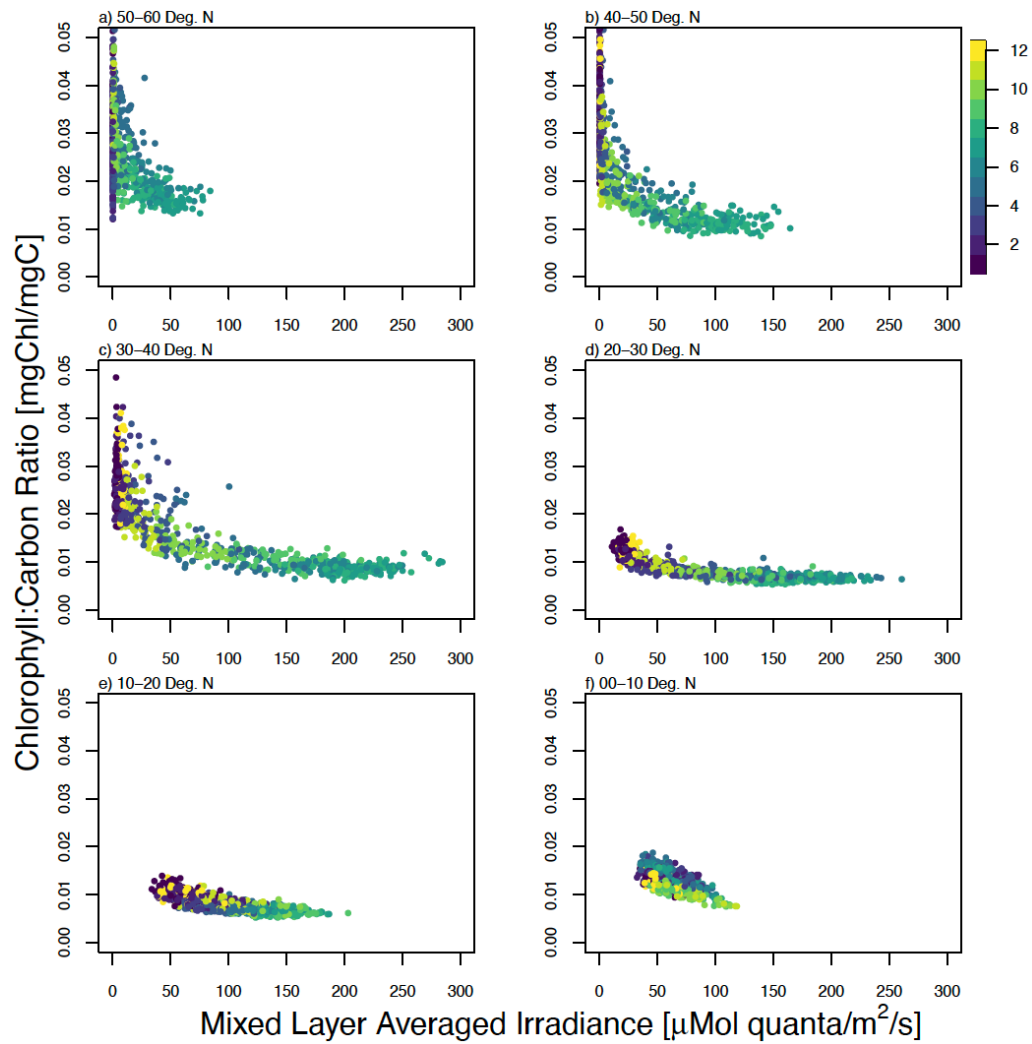


Figure S10. As in Figure 8 of the main text but using chlorophyll concentrations and backscatter coefficients estimated from the Garver-Siegel-Maritorena (GSM) ocean color inversion algorithm (Maritorena et al., 2002).